Journal of Chromatography A, 1218 (2011) 4632–4648

Contents lists available at ScienceDirect

Journal of Chromatography A

journal homepage: www.elsevier.com/locate/chroma

On the minimization of the band-broadening contributions of a modern, very high pressure liquid chromatograph

Fabrice Gritti, Georges Guiochon*

Department of Chemistry, University of Tennessee, Knoxville, TN 37996-1600, USA

ARTICLE INFO

Article history:
Received 28 January 2011
Received in revised form 6 May 2011
Accepted 9 May 2011
Available online 17 May 2011

Keywords:
Instrumentations
Band broadening
1290 Infinity HPLC system
Extra-column effects

ABSTRACT

The contributions of the volume of sample injected, the mobile phase flow rate, the inner diameter of the needle seat capillary and that of the connector capillary, the heat exchanger, and the detector cell volume to the widths of bands eluted from the 1290 Infinity HPLC instrument were investigated in depth. Four sample volumes (0.16, 0.80, 4.0, and 20 μL), three flow rates (0.04, 0.4, and 4.0 mL/min), two needle seat capillary I.D. (100 mm × 115 and 140 μm), three sets of connector capillary I.D. (350 mm × 80, 115, and 140 μm placed upstream the column, and 220 mm × 80, 115, and 140 μm downstream the column), two UV detector cell volumes (0.8 and 2.4 μL), and the presence/absence of the heat exchanger (1.6 μL) between the inlet connector capillary tube and the column were combined to generate up to 4 × 3 × 2 × 3 × 2 × 2 = 288 system configurations for this instrument. For each configuration, 5 consecutive injections were performed in order to assess the injection-to-injection repeatability, providing 1440 elution band profiles which are analyzed. The results demonstrate that the band broadening contribution of the instrument depends mostly on the detector cell volume and on the inner diameter of the needle seat capillary tube. The impact of these two contributions is particularly important at high flow rates (4 mL/min). Best efficiencies are obtained with a small sample volume, below 1 μL, which avoids volume overload of the instrument, or with large sample volumes, which maximize the radial concentration gradients of the sample across the instrument channels, in the vicinity of the anfractuosities of the channel walls. The injection of large sample volumes reveals the imperfection of current injection systems, the performance of which is remote from the one expected to provide an ideal rectangular injection (∼+4 μL^2). Although the present behavior of the instrument is satisfactory, serious improvements would become necessary to operate the next generation of more efficient columns that might be commercialized soon.

1. Introduction

The current trend towards the use of narrower bore (2 or even 1.0 mm I.D.) columns packed with sub-2 μm fully porous [1–3] or sub-3 μm superficially porous particles [4–12] has serious consequences on the design of HPLC instruments because it requires considerable efforts to limit extra-column band broadening. This shift is causing considerable, unexpected challenges to manufacturers of HPLC. The recent advent of a new generation of instruments able to operate under very high pressure [13] brings only partial answers to the problem by affording the possibility to operate the low permeability columns packed of sub-2 μm particles in a range of flow rates within which suitable compromises between column efficiency and analysis time can be selected. Yet, this progress in instrumentation does not always permit a full achievement of the potential of modern column technology for several reasons.

First, because modern columns are packed with fine particles they have lower permeabilities than conventional columns but their efficiencies peak at higher flow rates. So, they must be operated at high mobile phase velocities. The combination of this high velocity and of the high pressure gradient along the column results in the evolvement of an important amount of heat due to the combination of friction between the mobile phase and the particles and of the decompression of the mobile phase [14–19]. Radial diffusion of this heat causes a temperature gradient across the column, resulting in a measurable loss of column efficiency, even when the column is operated under still-air conditions [3,20–24]. Secondly, the volume of the bands eluted from these highly efficient columns is much smaller than that of bands eluted from traditional columns. Under isocratic conditions, which still represent a large proportion of the analyses that are made in industrial and research laboratories, the full performance of the modern, very efficient columns cannot be achieved by analysts due to instrument limitations [13,25].

* Corresponding author at: Department of Chemistry, University of Tennessee, 552 Buehler Hall, Knoxville, TN 37996-1600, USA. Tel.: +1 865 974 0733; fax: +1 865 974 2667.
E-mail addresses: guiochon@utk.edu, guiochon@ion.chem.utk.edu (G. Guiochon).

0021-9673/$ – see front matter © 2011 Elsevier B.V. All rights reserved.
doi:10.1016/j.chroma.2011.05.024

These limitations are caused by the extra-column band broadening contributions that arise everywhere in HPLC instruments, from the injection needle to the outlet of the detector cell. Ideally, the shape of sample plugs leaving the injector should be rectangular and the sample zone leaving a column should not have undergone any additional band broadening during its transit through the instrument channels. Unfortunately, the extra-column volumes of any instrument contribute to band broadening, significantly increasing the variances of the peaks eluted. With traditional instruments, these contributions are at least 50 μL^2 or even more; they are only of the order of 10 μL^2 for the most modern instruments [13]. Nevertheless, these variances considerably exceed the band variance of zones eluted from the most recent, very efficient 50 mm × 2.1 mm narrow-bore columns (hold-up volume V_0 = 100 μL, efficiency N = 15,000 plates) that are filled with the best packing materials now available. These bands have variances of a few μL^2 for poorly retained peaks (k = 1). Actually, the performance of the HPLC instruments currently available often does not permit to do justice to these modern columns. Important efforts, much ingenuity and resources must be invested to engineer more efficient instruments.

Different parts of the instruments contribute to broaden solute zones flowing from the injection needle to the detector outlet. The sample is drawn and stored inside a long capillary and into the injection loop. The rear part of this plug then diffuses at the interface between the sample solution and the eluent. The drawing speed being smaller than standard mobile phase flow rates, at ca. 20–100 μL/min may not affect much this contribution. Some systems are equipped with needle seat capillaries between the needle seat and the actuation valve, others are not and the loop is directly connected to the valve. When the needle seat capillary is present, once the switching valve is actuated, the sample zone if flushed in the opposite direction, toward the injection valve, a transfer made through the needle seat capillary. The sample zone is then transported through the inlet connector capillary, through the heat exchanger when necessary, through the outlet connector capillary, and, after elution through the column, through a last connecting tube into the detector cell. This cell consists in a short capillary tube (path length of 4–10 mm), which contributes to increase the sample bandwidth. Finally, the chromatogram is recorded by acquiring the signal at a constant sampling rate. These specific parts of the instrument are inter-connected using appropriate nuts, ferrules, and openings that generate many anfractuosities. All together, these connections and transfer parts contribute to broaden the sample zone, through mechanisms detailed later.

In this work, we quantified the impact of the characteristics (volume, diameter, eluent flow rate, signal sampling speed,...) of these different parts of an instrument to the observed extra-column band broadening, in the hope of pinpointing the critical parts of the system, the parts which should be improved to further minimize its extra-column band broadening contribution. For this purpose, we systematically measured the extra-column band profiles of samples of a dilute solution (C < 0.1 g/L) of naphthalene for 24 different configurations of extra-column channel in an Agilent 1290 Infinity system. Two needle seat capillaries I.D. (100 mm × 115 and 140 μm), three 350 mm long connecting tubes of I.D. of 80, 115, and 140 μm placed downstream the column, three 220 mm long connecting tubes of 80, 115, and 140 μm upstream the column, two UV detection cells of volumes 0.8 and 2.4 μL, and the presence/absence of the heat exchanger (1.6 μL) were combined, generating 2 × 3 × 2 × 2 = 24 combinations. Additionally, each system configuration was tested for four volumes of the injected sample (0.16, 0.80, 4.0, and 20.0 μL) and three eluent flow rates (0.04, 0.4, and 4.0 mL/min). Each measurement was repeated five times. A statistical analysis of the 1440 extra-column band profiles recorded is presented. The results indicate which parts of the 1290 Infinity system need most to be improved to provide the best results with the forthcoming narrow-bore columns packed with very fine particles. It is important to note that the quantitative results presented in this work concern exclusively the performance of the 1290 Infinity system used. However, from a qualitative viewpoint, the general conclusions are valid for other vHPLC instruments, which operate similarly.

2. Theory

2.1. First moments of extra-column peaks

The volumes of the injected sample (V_{Vnj}), the needle seat capillary (V_{Seat}), the injection valve (V_{Valve}), the connecting tubes (V_{Cap}), the heat exchanger (V_{Heat}), the UV detector cell (V_{Cell}), and the volume contribution of the sampling rate (τF_v) are known. τ is the sampling time and F_v is the flow rate. These parameters and their values are listed in Table 1. The extra-column contribution to the first moment of the bands, $\mu_{1,v,Ex}$, expected in the absence of sample dispersion (no flow heterogeneity in any part) is given by:

$$\mu_{1,v,Ex} = \frac{V_{Inj}}{2} + V_{Seat} + V_{Valve} + V_{Cap} + V_{Heat} + \frac{V_{Cell}}{2} + \frac{\tau F_v}{2} \quad (1)$$

However, the volume of the anfractuosities present along the instrument channels and the slow diffusive mass transfer into and out of them contribute to increase further the hold-up volume of the instrument and causes a degree of tailing. For these reasons, the first moments observed are slightly larger than expected.

2.2. Second moments of extra-column peaks

The different parts of the instrument that contribute to the dispersion of a sample band include the system drawing the sample from the vial into the injection loop and ejecting it into the needle seat, $\sigma^2_{v,Inj}$, the volume of the injected sample itself, σ^2_{v,V_i}, the needle seat capillary, $\sigma^2_{v,Seat}$, the injection valve, $\sigma^2_{v,Val}$, the tubes connect-

Table 1
First moments including the contributions of the injection volume, needle seat capillary, injection valve, connecting tubes, detection cell volume, and sampling rate.

			First moment [μL]
Injection volume [μL]	0.16		0.08
	0.80		0.40
	4.00		2.00
	20.00		10.00
Injection valve			1.2 [a]
	L [cm]	I.D. [μm]	
Needle seat length × I.D.	10	115	1.04
	10	140	1.54
Heat exchanger			1.6 [a]
Connecting tubes length × I.D.	22	80	1.11
	22	115	2.29
	22	140	3.39
	34	80	1.71
	34	115	3.53
	34	140	5.23
Detection cell volume [μL]	0.8		0.40
	2.4		1.20
Sampling rate [Hz]/flow rate [mL/min]	40		0.01
	0.04		
	80		0.04
	0.4		
	160		0.21
	4.0		

[a] Data provided by the manufacturer.

ing the valve to the column and the column to the detector, $\sigma^2_{v,Cap}$, the detector cell, $\sigma^2_{v,Cell}$, the heat exchanger, $\sigma^2_{v,Heat}$, the sampling rate, $\sigma^2_{v,Rate}$, and the contributions of mass transfer into and out of all the unavoidable anfractuosities along these parts and at their connection points, $\sigma^2_{v,Nooks}$.

Therefore, if we assume that the variances of these different sources of band broadening are additive (which is in practice barely the case), the total extra-column peak variance, $\sigma^2_{v,Ex.}$, in volume unit is written:

$$\sigma^2_{v,Ex.} = \sigma^2_{v,Inj} + \sigma^2_{v,V_i} + \sigma^2_{v,Seat} + \sigma^2_{v,Val} + \sigma^2_{v,Cap} + \sigma^2_{v,Heat} + \sigma^2_{v,Cell} + \sigma^2_{v,Rate} + \sigma^2_{v,Nooks} \quad (2)$$

Some of these contributions to the total extra-column peak variance have been quantified formerly; their estimates are well known [26]. The other contributions can be modeled and algebraic expressions derived to predict the values of σ^2_{v,V_i}, $\sigma^2_{v,Seat}$, $\sigma^2_{v,Cap}$, $\sigma^2_{v,Cell}$, and $\sigma^2_{v,Rate}$ are detailed below. These expressions do not necessarily account for the true observed band variance but serve as reference values.

2.2.1. Short cylindrical tubes

The contribution of connecting tubes is based on the coupling [27] between the asymptotic Aris dispersion theory in open tubular tubes [28] and a flow dispersion regime assuming a radial, Hagen–Poiseuille parabolic flow profile [29]. The set of tubes includes the needle seat capillary ($\sigma^2_{v,Seat}$) and the several connecting tubes ($\sigma^2_{v,Cap}$), those between the injection needle and the heat exchanger, the heat exchanger and the column inlet, the column outlet and the detector.

The asymptotic variance in volume unit predicted by Aris when the band center has reached the end of a cylindrical tube of length L and inner radius r_c is [28]:

$$\sigma^2_{v,Cap,Aris} = \frac{1}{24}\frac{\pi r_c^4 L}{D_m} F_v \quad (3)$$

where D_m is the bulk molecular diffusion coefficient ($D_m = 1.26 \times 10^{-5}$ cm^2/s for naphthalene, in a mixture of acetonitrile and water, 80/20, v/v, at 293.15 K [30]) and F_v is the flow rate. This expression applies only for infinitely long tubes and/or infinitely small flow rates. It does not apply to the actual needle seat capillary tube nor to the connecting tubes.

The variance in volume when the band center has reached the end of the cylindrical tube of length L, assuming a radial parabolic flow profile and no radial diffusion is given by [29]:

$$\sigma^2_{v,Cap,Flow} = \frac{1}{3}\pi^2 r_c^4 L^2 \quad (4)$$

The coupling theory of eddy dispersion of Giddings provides the variance contribution, $\sigma^2_{v,Tube}$, of an open cylindrical tube of inner radius r_c when the band center has reached the length $z = L$ is given by [31]:

$$\sigma^2_{v,Cap} = \frac{\pi^2 r_c^4 L^2}{3 + (24\pi L D_m / F_v)} \quad (5)$$

2.2.2. Injection volume

The contribution of the injected volume, V_{inj}, to the extra-column band broadening is given by [26]:

$$\sigma^2_{v,V_i} = \frac{V^2_{Inj}}{12} \quad (6)$$

2.2.3. Detection cell volume

The contribution of the volume of the UV detector cell, V_{cell}, to the extra-column band broadening is also given by:

$$\sigma^2_{v,Cell} = \frac{V^2_{Cell}}{K} \quad (7)$$

In practice, the factor $K = 12$ is not a physically realistic value. Usually, K lies between 1 (ideal mixer) and 12 (non-dispersive cell). Values of 5–6 are more generally correct. Note that this variance is independent of the flow rate applied.

2.2.4. Sampling rate

The contribution of the detector time constant or, for modern systems, its sampling rate is proportional to the product of the time constant, τ, by the flow rate squared [26,27]:

$$\sigma^2_{v,Rate} = \frac{1}{12}\tau^2 F_v^2 \quad (8)$$

This expression assumes that the signal observed at time t, $I(t)$, is the average of the real signal, $s(t)$, over the time interval $t - \tau$ to t or:

$$I(t) = \frac{1}{\tau}\int_{t-\tau}^{t} s(t')\,dt' \quad (9)$$

Table 2 lists the expected values of σ^2_{v,V_i}, $\sigma^2_{v,Seat}$, $\sigma^2_{v,Cap}$, $\sigma^2_{v,Cell}$, and $\sigma^2_{v,Rate}$ for the four injection volumes used (0.16, 0.80, 4.0, and 20 μL) and the three flow rates (0.04, 0.4, 4.0 mL/min).

2.2.5. Unknown variance contributions

The contributions $\sigma^2_{v,Inj}$ of the injection sequence (drawing and ejection of the sample volume), $\sigma^2_{v,Val}$ of the injection valve, $\sigma^2_{v,Heat}$ of the zig-zag heat exchanger capillary, and $\sigma^2_{v,Nooks}$ of all the anfractuosities in the LC system cannot be calculated a priori and are unknown *a priori*.

3. Experimental

3.1. Chemicals

The mobile phase used in this work was a mixture of acetonitrile and water (80/20, v/v). Both solvents were HPLC grade from Fisher Scientific (Fair Lawn, NJ, USA). The mobile phase was filtered before use on a surfactant-free cellulose acetate filter membrane, 0.2 μm pore size (Suwannee, GA, USA). The sample naphthalene was also purchased from Fisher Scientific.

3.2. Apparatus

The 1290 Infinity HPLC system (Agilent Technologies, Waldbroon, Germany) was used in this work. This instrument includes a 1290 Infinity Binary Pump with Solvent Selection Valves and a programmable auto-sampler. The injection volumes were set at 0.16, 0.80, 4.0, and 20 μL. The flow rates were successively set at 0.04, 0.4, and 4.0 mL/min. The instrument is equipped with a two-compartment oven and a multi-diode array UV–vis detection system. The sampling rates of the detector were fixed at 40 Hz (for a flow rate of 0.04 mL/min), 80 Hz (for $F_v = 0.4$ mL/min), and 160 Hz (for $F_v = 4.0$ mL/min). The system is controlled by the Chemstation software. The sample migration throughout the equipment involves its successive passage through the following series of channels

Table 2
Prediction of some system variances in μL^2 including the contributions of the injection volume, needle seat capillary, connecting tubes, detection cell volume, and sampling rate.

V_{inj} [μL]			0.16			0.8			4			20		
Flow rate [mL/min]		0.04	0.4	4	0.04	0.4	4	0.04	0.4	4	0.04	0.4	4	
Sampling rate [Hz]		40	80	160	40	80	160	40	80	160	40	80	160	
	L [cm]	I.D. [μm]	Second central moment [μL^2]											
Needle seats length × I.D.	10	115	0.36	0.36	0.36	0.36	0.36	0.36	0.36	0.36	0.36	0.36	0.36	0.36
	10	140	0.79	0.79	0.79	0.79	0.79	0.79	0.79	0.79	0.79	0.79	0.79	0.79
Connecting tubes length × I.D.	22	80	0.41	0.41	0.41	0.41	0.41	0.41	0.41	0.41	0.41	0.41	0.41	0.41
	22	115	1.74	1.74	1.74	1.74	1.74	1.74	1.74	1.74	1.74	1.74	1.74	1.74
	22	140	3.81	3.82	3.82	3.81	3.82	3.82	3.81	3.82	3.82	3.81	3.82	3.82
	34	80	0.97	0.97	0.97	0.97	0.97	0.97	0.97	0.97	0.97	0.97	0.97	0.97
	34	115	4.16	4.16	4.16	4.16	4.16	4.16	4.16	4.16	4.16	4.16	4.16	4.16
	34	140	9.13	9.13	9.13	9.13	9.13	9.13	9.13	9.13	9.13	9.13	9.13	9.13
Injection volume			0.00	0.00	0.00	0.05	0.05	0.05	1.33	1.33	1.33	33.33	33.33	33.33
Detection cell volume [μL]	0.8		0.05	0.05	0.05	0.05	0.05	0.05	0.05	0.05	0.05	0.05	0.05	0.05
	2.4		0.48	0.48	0.48	0.48	0.48	0.48	0.48	0.48	0.48	0.48	0.48	0.48
Sampling			0.00	0.00	0.01	0.00	0.00	0.01	0.00	0.00	0.01	0.00	0.00	0.01

- A 20 μL injection loop attached to the injection needle (note that the whole 20 μL is not flushed with the sample).
- A 100 mm long needle seat capillary between the injection needle and the injection valve.
- An injection valve. The total volume of the grooves and connection ports in the valve is around 1.2 μL.
- Two connector capillaries, the first being 340 mm long (before the heat exchanger) and the second 220 mm long (after the column and before the detector cell).
- The heat exchanger capillary, volume 1.6 μL.
- The column, replaced in this study with a zero-volume connector (ZDV, actual volume ca. 0.1 μL, I.D. 1/48 in. or ca. 0.52 mm, length 0.5 mm).
- A small volume detector cell, path length 10 mm.

Table 1 lists the dimensions of the two needle seat capillaries, the diameters of the six connecting tube capillaries, and the volumes of the two detector cells used in this work. Note that the 0.8 μL detection cell is not commercially available (prototype cell).

The flow rate accuracy was determined by directly pumping the pure mobile phase at 295 K and 1 mL/min during 50 min into a volumetric flask of 50 mL in the absence of chromatographic column. The eluent was collected at the exit of the heat exchanger of the chromatograph. The relative error was less than 0.2%, so we estimate that the long-term accuracy of the flow-rate at 1 mL/min is around 2 μL/min. The laboratory temperature was controlled by an air conditioning system set at 293 K. The daily variation of the ambient temperature never exceeded ±1 °C.

3.3. Samples

The sample naphthalene was dissolved in the eluent mixture (<0.1 g/L). A 10 mL sample was prepared and stored in a refrigerator at 277 K. The concentration was set low enough in order to observe a maximum UV signal of 1700 mAU and a linear response of the detector when 20 μL samples were injected. The wavelength of the UV detector was set at 254 nm with a bandwidth of 4 nm. Naphthalene dissolved in a mixture of acetonitrile and water (80/20, v/v) was chosen because its diffusion coefficient is typical of those of small molecular weight compounds dissolved in the standard eluents ($\simeq 1–2 \times 10^{-5}$ cm^2/s) used for quality control tests of vHPLC columns.

3.4. Experimental plan

The 1290 Infinity system was operated with 24 successive configurations characterized by the choice made for the inner diameters of the needle seat capillary and the connecting capillary tubes, for the volume of the detector cell and for the presence/absence of the heat exchanger. For each configuration of the system, three different flow rates were considered. At each flow rate, four injected volumes were applied. Thus, a total of 288 different injections were performed, each being repeated five times. This makes a total of 1440 injections.

3.5. Measurements of the first moment and the second central moment

The extra-column contributions to the retention volume and the band broadening of the probe samples were measured by replacing the chromatographic column with a ZDV union connector. The extra-column retention volumes and variances were measured using the only accurate method available, the numerical integration method [32]. Each measurement was repeated five times. Prior to any measurement, each profile recorded was cut on its left and right sides and corrected for baseline drift. The left and right cut-off abscissa were determined when the positive (left side) and negative (right side) drifts of the signal were smaller than the noise of the signal. This determination of when the integration of the signal should begin and end is critical for the precision of the measurements [33]. The higher the order of the moment, the larger the contribution of the parts of the peak that are remote from its center, hence the larger the influence of the signal noise.

The first moment and the second central moment of the concentration profiles of the sample were calculated by dumping the set of recorded data into a 2-column (time and signal) MS Excell spreadsheet and using the following formulae to derive the moments (NB. The moments provided by the data station were not used):

$$\mu_1 = \frac{\sum_{i=1}^{i=N-1} (C_i + C_{i+1})(t_i + t_{i+1})}{2\sum_{i=1}^{i=N-1} C_i + C_{i+1}} \quad (10)$$

$$\mu_2' = \frac{\sum_{i=1}^{i=N-1} (C_i + C_{i+1})((t_i + t_{i+1}/2) - \mu_1)^2}{\sum_{i=1}^{i=N-1} C_i + C_{i+1}} \quad (11)$$

where N is the number of data points (t_i, C_i) left after elimination of the early and late recorded data points (see above). The first and second moments of the sample peak, $\mu_{1,j}$ and $\mu_{2,j}'$, were determined successively five times (j = 1–5). The averages, $\overline{\mu_1}$ and $\overline{\mu_2'}$, and their relative sample standard deviations, σ_{n-1,μ_1} and $\sigma_{n-1,\mu_2'}$ were calculated as follows, using the same method as for the sample peak:

$$\overline{\mu_1} = \frac{1}{5}\sum_{j=1}^{j=5} \mu_{1,j} \quad (12)$$

$$\overline{\mu_2'} = \frac{1}{5}\sum_{j=1}^{j=5} \mu_{2,j}' \quad (13)$$

$$\sigma_{n-1,\mu_1} = \frac{\sqrt{1/4\sum_{j=1}^{j=5}\left(\mu_{1,j} - \overline{\mu_1}\right)^2}}{\overline{\mu_1}} \quad (14)$$

$$\sigma_{n-1,\mu_2'} = \frac{\sqrt{1/4\sum_{j=1}^{j=5}\left(\mu_{2,j}' - \overline{\mu_2'}\right)^2}}{\overline{\mu_2'}} \quad (15)$$

4. Results and discussion

The precision of our measurements of the extra-column contributions are first analyzed and discussed. Then, the impact of each of the experimental parameters studied (injection volume, flow rate, needle seat capillary, connecting tube capillaries, heat exchanger, and detection cell) on the overall band broadening is investigated and discussed. The goal of this section is to elucidate under which conditions one or several of these parameters together control most of the band spreading taking place during migration of the analyte band along the channel of the instrument. Finally, this analysis leads to suggesting what are the most important and most practical solutions to improve an HPLC system in order to achieve satisfactory performance with the new, short narrow-bore 2.1 mm I.D. columns.

4.1. Precision of the experimental data

The second and first moments of the extra-column peak, μ_2' and μ_1, were measured successively five times each. The relative standard deviations of these measurements are plotted in Figs. 1 (first moment) and 3 (peak variance). The sub-divisions of the x-axis in these figures are organized as follows: in the first position, the injected volume (0.16, 0.80, 4.0, and 20 μL from left-to-right); in the second position, the flow rate (0.04, 0.4, and 4.0 mL/min from left-to-right); in the third position, the I.D. of the needle seat capillary (115 and 140 μm from left-to-right); in the fourth position, the I.D. of the connecting tube capillary tubes (80, 115, and 140 μm from left-to-right); in the fifth position, the volume of the detection cell (0.8 and 2.4 μL from left-to-right); and in the sixth and last position, the presence (left) or absence (right) of the zig-zag heat exchanger capillary tube.

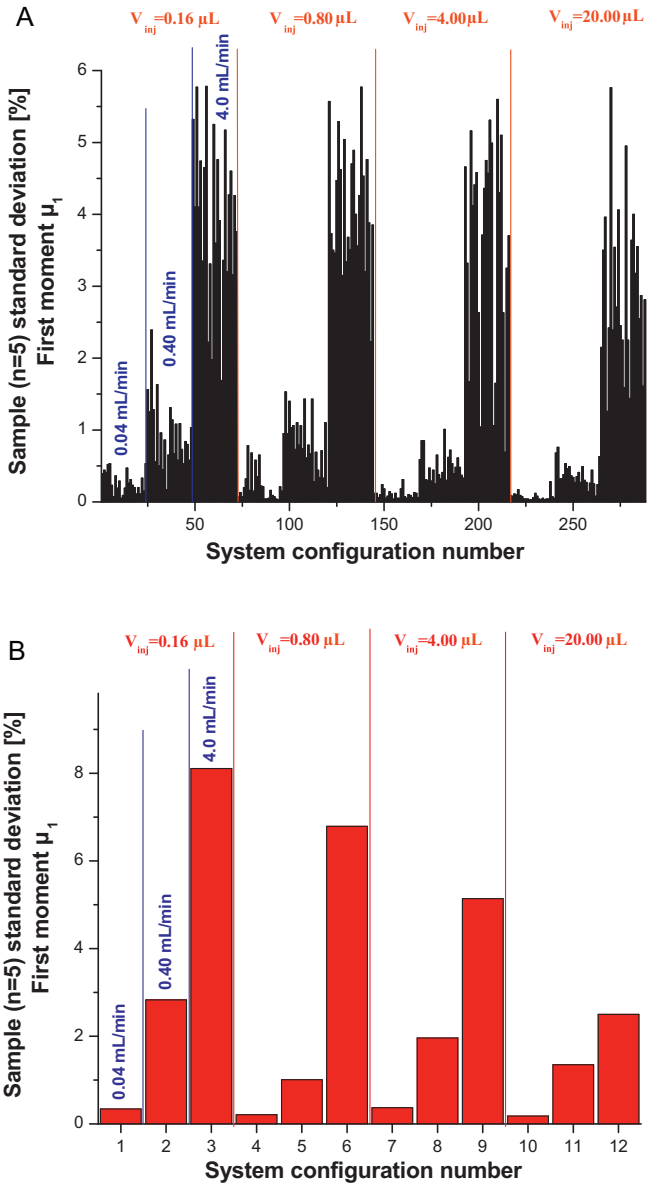

Fig. 1. (A) Injection-to-injection repeatability of the first moments. Plot of the sample (n = 5) relative standard deviation (RSD) of the first moment of the extra-column band profiles as a function of the 288 system configurations. The x-axis is successively divided into 4 injection volumes, 3 flow rates, 2 needle seat capillary I.D., 3 connecting capillary tube I.D., 2 detection cell volumes, and presence/absence of the heat exchanger). (B) Sequence-to-sequence repeatability after unfastening and fastening all connections. Note the major impact of the flow rate on the precision of the data.

We analyze the injection-to-injection and the sequence-to-sequence repeatabilities of the first and second central moments. In the sequence-to-sequence repeatability experiments, all the parts of the 1290 system were removed before being assembled as required and all the units of the chromatograph (pump, sample manager, and detection) were completely turned off.

4.1.1. Injection-to-injection precision of the first moment

Fig. 1A demonstrates that the precision of the measurements of the first moments depends mostly on the flow rate applied and slightly on the volume injected. At a constant flow rate of 0.04 mL/min, the average RSDs of the $\mu_{1,j}$ measurements are 0.28%, 0.23%, 0.11%, and 0.07% for injected volumes of 0.16, 0.80, 4.00, and 20.0 μL, respectively. The same RSDs are 0.94%, 0.85%, 0.50%, and 0.38% for the 10-fold larger flow rate of 0.4 mL/min, the relative

errors becoming 3–5 times larger. Finally, at a constant flow rate of 4.0 mL/min, the average RSDs are equal to 4.12%, 4.01%, 3.64%, and 2.95%, between 15 and 20 times larger than those recorded at the lowest flow rate.

We investigated whether a time offset between the moment when the injection valve is actuated and the moment when the detector records the initial time ($t = 0$) could account for this observation. The plot of the elution volume $F_v\mu_1$ *versus* the flow rate F_v reveals a slight convex upward shape with an average slope of 0.055 s (±30%) for all the 24 configurations tested in this work. If we consider the system configuration with the lowest volume, this offset time accounts for 0.4, 3.8, and 32.0% of the elution time of a 0.8 μL injection at flow rates of 0.04, 0.4, and 4.0 mL/min, respectively. Given the 30% random dispersion around the mean value of 0.055 s, an increase of the RSDs of the $\mu_{1,j}$ measurements would be consistent with the existence of a variable offset time in between 0.038 and 0.072 s. In addition, the sample injection itself causes a pressure disturbance, hence a flow disturbance. The larger the flow rate, the higher the pressure and the larger the erratic flow disturbance.

Everything else being constant, the RSDs of the first moments decrease with increasing sample size. Fig. 2A shows the variation of the average RSDs of $\mu_{1,j}$ as a function of the injected volume. There is no obvious physical explanation for this effect that is certainly not related to a variation of the elution times with increasing sample size (see later). We note that the relative decrease of the RSDs is particularly rapid with the smallest sample size and much less with the largest one. This could suggest that the repeatability of elution times is more robust at high than at low concentrations, i.e., when the concentration gradients in the system are the largest.

Fig. 2B shows the superimposition of the four chromatograms recorded at a flow rate of 0.4 mL/min, under the same conditions (see caption). Clearly, the concentration distributions along the channels differ significantly from one injection volume to the next, varying in a 5-fold ratio between 0.16 and 0.80 μL and only in a 1.6-fold ratio between 4.0 and 20 μL. The lowest signal-to-noise ratios observed for a 0.16 μL injection volume are 600, 500, and 350 at flow rates of 0.04, 0.4, and 4.0 mL/min, respectively. These observations explain the decreasing trends of the plots in Fig. 2A, which are most likely related to the intensity of the concentration gradients inside the tubes. As stated earlier, this trend is not related to a variation of the elution time, as confirmed by the constancy of the positional of the peak apex, 1.68 *v* ersus 1.69 second when the sample volume is increased from 0.16 to 0.80 μL.

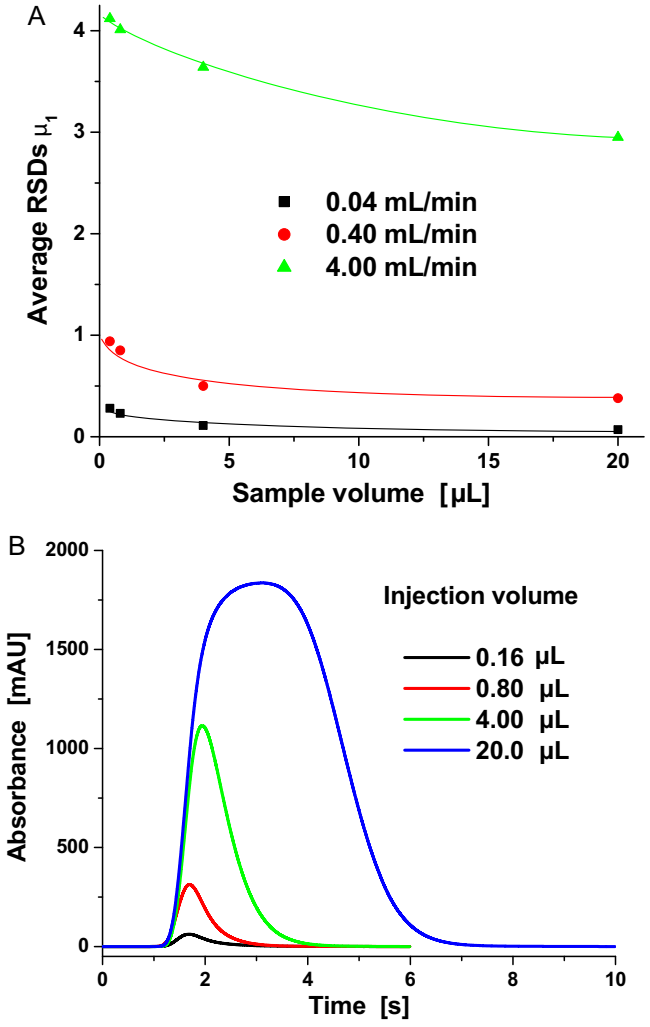

Fig. 2. (A) Plot of the average RSDs of the first moment measured at three different flow rates as a function of the injected sample volume. Note the large sensitivity of the precision in the range of small injection volumes (0 → 7 μL). (B) Superimposition of the extra-column band profiles recorded for a series of injection volumes as indicated in the legend. Conditions: 115 μm I.D. needle seat capillary, 80 μm I.D. connecting tubes, 2.4 μL detector cell, and the heat exchanger present. Note that the signal height does not increase linearly with increasing sample volume only the peak area does.

4.1.2. Injection-to-injection precision of the second moment

Fig. 3A reports on the RSDs of the second central moment, $\mu'_{2,j}$, of the sample peak for all the 288 system configurations used. In contrast to the RSDs measured for the first moment $\mu_{1,j}$, the precision of the experimental second moments is mostly controlled by the sample volume injected. The dependence of the volume variance on the sample volume was investigated long ago with prototypes of the 1090 Agilent instrument [34]. Fig. 4 shows plots of the average RSDs of the second central moments as a function of the sample volume. The decreasing trend of these RSDs with increasing sample volume is stronger than the one reported in Fig. 2A for the first moment. The average RSDs decrease from 3.07% to 1.43%, 1.01% and 0.20% at a flow rate of 0.04 mL/min, from 4.82% to 2.71%, 0.72% and 0.29% at 0.4 mL/min, and from 6.31% to 2.46%, 1.22% and 0.81% at 4.0 mL/min when the volume injected increases from 0.16 to 0.80, 4.00 and 20.0 μL, respectively. Clearly, more than on anything else, the precision of the second central moment depends strongly on the sample volume, e.g. on the intensity of the concentration gradients migrating along the extra-column volumes. Less obvious but still measurable, the precision of the second moment increases with decreasing flow rate.

4.1.3. Sequence-to-sequence precision

During the series of experiments performed in this work, some parts were removed from and others were installed onto the 1290 Infinity system. This requires to fasten/unfasten a significant number of end-fittings to change the needle seat capillary I.D., the connecting tubes I.D., and/or to replace the heat exchanger with a union connector. At the same time, at the end of each sequence, the pump, the sample manager, and the detector modulus were systematically turned off.

Accordingly, a sequence-to-sequence repeatability test was performed by repeating the measurement of the first and second central moments after disconnecting each part (needle seat capillary, two connecting tubes, heat exchanger, union connector, and detection cell), unfastening 6 different screws and turning off the whole 1290 Infinity system. The results are shown in Fig. 1B (first moments) and in Fig. 3B (second central moments). They confirm that the precision of the first and second central moment depends mostly on the flow rate (random offset time) and on the volume injected (e.g. the amplitude of the concentration gradients), respectively. However, a comparison of Figs. 1 and 3 shows

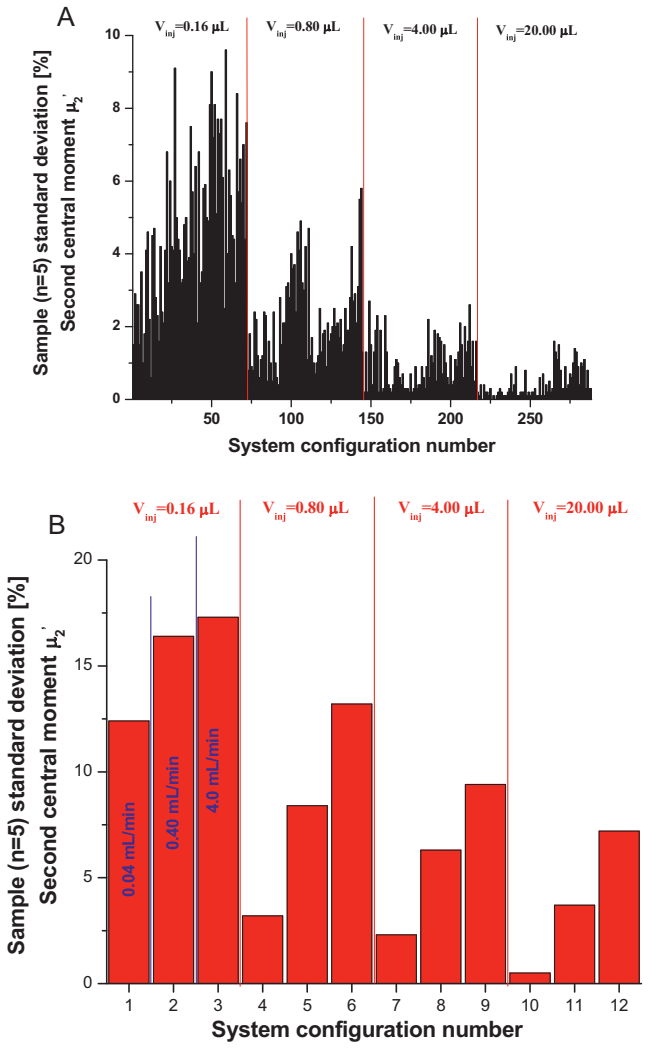

Fig. 3. Same as in Fig. 1, except the injection-to-injection repeatability of the second central moments of the extra-column band profiles. Note the major impact of the sample volume injected.

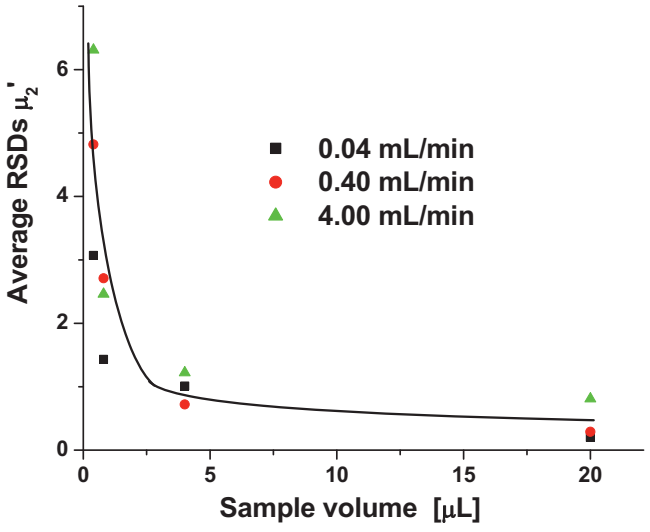

Fig. 4. Plot of the average RSDs of the second central moments measured at three different flow rates as a function of the injected sample volume. Note the very large sensitivity of the precision in the range of small injection volumes (0 → 4 µL).

a larger sequence-to-sequence RSDs than injection-to-injection RSDs. Overall, the maximum RSDs were found equal to 8% for the first moment and 17% for the second central moment (0.16 µL injected, 4 mL/min). The smallest RSDs were 0.18% and 0.50% at a flow rate of 0.04 mL/min and an injection volume of 20 µL.

4.1.4. Conclusion on the precision

On the average over the 24 system configurations, the injection-to-injection relative errors made on the first moments vary between 0.1% (low flow rate and high concentration gradients) and 4.0% (high flow rate and small concentration gradients). The same relative errors for the second central moments range between 0.2% (high concentration gradients and low flow rate) and 6.5% (small concentration gradients and high flow rates). The precision of the integration method depends essentially on the reproducibility of the beginning and the end of the integration of the signal, i.e., of the left and right cut-off abscissa. The largest relative errors of 4% and 6.5% for the first moments and the second central moments, respectively, may appear large. The largest sequence-to-sequence errors are somehow larger, at 8% for the first moment and 17% for the second central moment.

Yet, it is important to underline that these moments were measured based on a full numerical integration method, as described in the experimental section and previously analyzed elsewhere [32]. As shown earlier, the results of this method are highly sensitive to the noise in the regions where the solute concentrations are the lowest and where the degree of repeatability is the smallest. The error made depends much on the times when the integration begins and ends, i.e., on the positions of the far-left and far-right cut-off points [33]. Thus, this method is less robust than others, such as the half-height peak width and/or the peak fitting methods. In contrast, the numerical integration method has the great advantage of providing far more accurate measurements of the first and second central moments, which is why we used it.

Finally, we should emphasize that only the excellent repeatability of the performance of the injection system of the 1290 Infinity system allows the achievement of the high level of injection-to-injection reproducibility that was consistently obtained in this work.

4.2. Analysis of the first moment of the extra-column band profiles

Fig. 5A shows the averages of the first moments of the signals acquired for all the samples injected on the 288 system configurations outlined earlier. Fig. 5C zooms in to the 24 system configurations (2 needle seat capillary I.D., 3 connecting tube capillary's I.D., 2 detection cell volumes, and presence/absence of the heat exchanger), for a sample volume of 0.16 µL and a flow rate of 0.04 mL/min. This was the combination of sample size and flow rate giving the smallest average relative error for the first moment, at less than 0.3%.

Interestingly, we can identify the repetition of the same pattern in Fig. 5A for all the combinations (12) of flow rates and sample volumes. Fig. 5B compares the experimental and predicted first moments based on the estimates of the geometrical volumes of the different parts of the 1290 Infinity system described earlier (Table 1). The detailed pattern observed at constant sample volume and flow rate shown in Fig. 5C reveals the impact of the different parts of the chromatographic system on the elution volume. The effects of the presence/absence of the heat exchanger (1.6 µL), of the detection cell's volume (0.8 or 2.4 µL), of the I.D. of the connecting tube capillaries (80, 115, or 140 µm), and of the I.D. of the needle seat capillary (115 or 140 µm) are clearly illustrated in this figure.

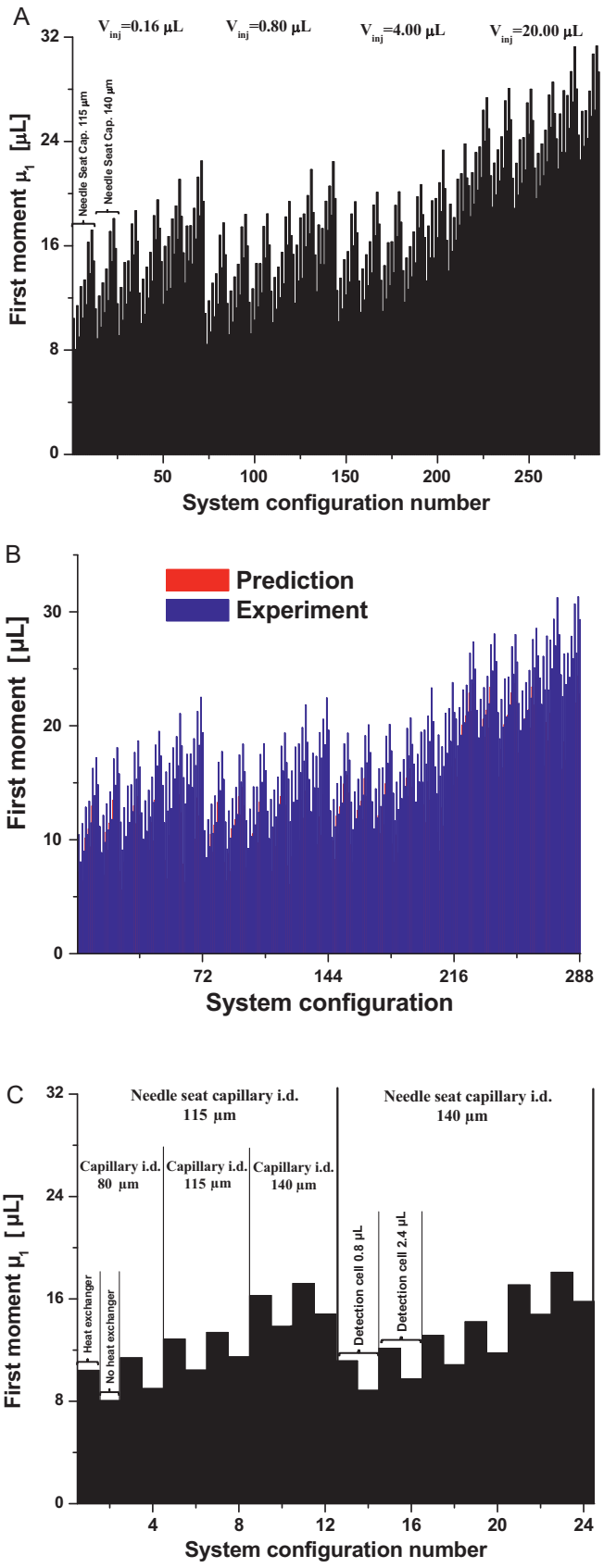

Fig. 5. (A) Plot of the first moments measured for the 288 system configurations. The *x*-axis is successively divided into 4 injection volumes, 3 flow rates, 2 needle seat capillary I.D., 3 connecting capillary tube I.D., 2 detection cell volumes, and the presence/absence of the heat exchanger. (B) Comparison between the observed and predicted first moments of the extra-column band profiles of the 1290 Infinity system. (C) Zoom in for a constant injection volume (0.16 µL) and a flow rate (0.04 mL/min) showing more clearly the contributions of the needle seat capillary I.D., the connecting tube capillary I.D., the detection cell volume, and the presence or absence of the heat exchanger along the extra-column path.

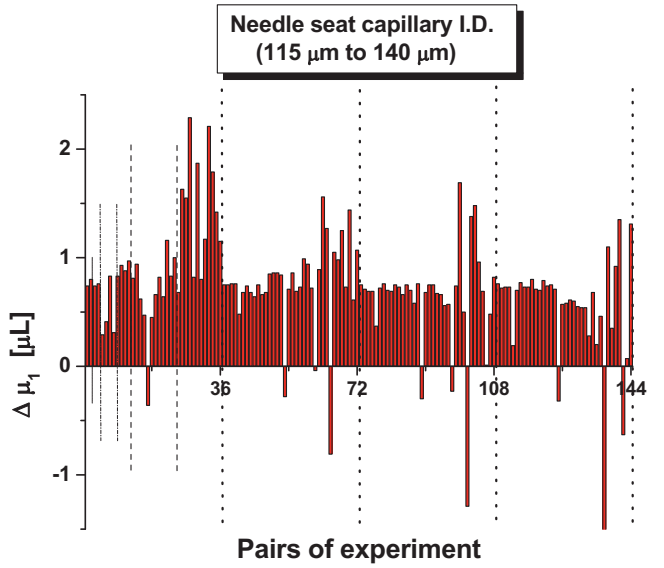

Fig. 6. Impact of increasing the I.D. of the needle seat capillary from 115 to 140 µm for 144 system configurations on the first moment observed. The *x*-axis is successively divided into 4 injection volumes, 3 flow rates, 3 connecting tube I.D., 2 detection cell volumes, and the presence/absence of the heat exchanger. The average increase in the first moment is 0.72 µL.

We observe that the elution volume in Fig. 5B is systematically about 30% larger than the sum of all the geometrical contributions listed in Table 1. For instance, the smallest elution volume, 8.05 ± 0.03 µL, was measured with a 0.16 µL injection volume, a 0.04 mL/min flow rate, a 115 µm needle seat capillary I.D., a 80 µm connecting tube I.D., a 0.8 µL detection cell, in absence of the heat exchanger. In contrast the sum of the volumes of all these parts is equal to 5.55 µL. The largest elution volume, 31.3 ± 0.9 µL, was measured with a 20.0 µL injection volume, a 4 mL/min flow rate, a 140 µm needle seat capillary I.D., a 140 µm connecting tube I.D., a 2.4 µL detection cell, in the presence of the heat exchanger. The sum of the volumes given in Table 1 gives a value of 24.4 µL. This confirms that the contributions of the unidentified parts of the injection system, the complex radial flow distribution and the anfractuosities along the channels of the extra-column volume is causing a significant delay in the elution volume of the bands of naphthalene. This difference is not due to a time off-set between the moments when the sample is physically injected and the zero time of the data station (as the off-set time of 0.6 second previously observed with the Acquity chromatograph [17]) but it is due to a significant contribution of channel anfractuosities and amount of peak tailing.

Next, we assess the contribution of each specific part of the instrument (needle seat capillary I.D., connecting tubes capillaries I.D., presence/absence of heat exchanger, detection cell volume, injection volume, and flow rate) by measuring the difference between two first moments recorded under the very same experimental conditions, except for one particular characteristic (I.D., volume, presence/absence) of one single instrument's part.

4.2.1. Needle seat capillary I.D. and μ_1

Fig. 6 shows the differences between the elution volumes of naphthalene when the instrument is fitted with the 140 or with the 115 µm I.D. needle seat capillary tube. 144 pairs of system config-

urations were considered in each case. From left to right, the *x*-axis represents the injected volume (4 segments including 36 pairs of experiment, see the dotted lines in Fig. 6), the flow rate (3 segments including 12 pairs of experiment, see the dashed segments in the same figure), the I.D. of the connecting tubes (3 segments including 4 pairs of experiment, see the dash-dotted lines in the same figure), the volume of the detection cell (2 segments including 2 pairs of experiments, see the short dotted line in the same figure), and the presence/absence of the heat exchanger (last two pairs of experiment).

As could be expected, most pairs of experiments generate a positive difference (134 out of a total of 144). Also noticeable is that all four unexpected negative outcomes (−0.35 μL) were observed for the same system configuration (0.4 mL/min, 115 μm I.D. connecting tubes, detection cell volume 0.8 μL, heat exchanger present) for each injected volume. The six other negative values were found to be random but always at the highest flow rate of 4.0 mL/min, where the precision of the measurements is largest, between 3% and 4%. At such a high flow rate, the limited precision of the synchronization between the injection valve, the detector, and the Chemstation have a large impact on the repeatability of the measurements.

Overall, the average difference between the elution volumes is 0.72 μL while the difference in the geometrical volume between the two needle seat capillaries is 0.50 μL (see Table 1). This could suggest either that there are wide variations of the inner diameter of the needle seat capillary tube around the specification or that increasing the needle seat capillary diameter enhances peak tailing. The capillary diameter tolerances are in the order of ±10% so that the volume difference could be ±20%, slightly more than half the difference observed.

4.2.2. Connecting tube capillary I.D. and μ_1

Fig. 7A shows the differences between the experimental elution volume observed with the 115 and the 80 μm I.D. connecting capillary tubes. Fig. 7B shows a plot similar to the one in Fig. 7A, for the 140 and 115 μm I.D. connecting capillary tubes. 96 different pairs of system configurations are available (4 samples volumes, 3 flow rates, 2 needle seat capillaries, 2 detection cells, and the presence or absence of the heat exchanger). Their differences are illustrated by using different styles to draw lines in these two figures.

With no exception, the differences in elution volumes are all positive and the sample relative standard deviation around the mean is much smaller (n = 96, RSD = 19 and 16%) than that observed in the previous section (n = 144, RSD = 72%), probably because the total length of the connecting tubes (560 mm) is much longer than that of the needle seat capillary (100 mm). The average increases of the first moment are 2.08 and 3.52 μL in Fig. 7A and B, respectively. Actually, the differences between the geometrical volumes of these three connecting tubes are $(2.29-1.11)+(3.53-1.71)=3.00$ μL and $(3.39-2.29)+(5.23-3.53)=2.80$ μL, according to Table 1. Clearly, the experimental differences is not the same as the one expected from the differences of the geometrical volumes of the connecting tubes provided by the manufacturer. Again, as was found with needle seat capillary I.D., either there are wide fluctuations of the inner diameter of the connecting tubes or the extent of peak tailing strongly depends on the inner diameter of these tubes.

4.2.3. Detection cell volume and μ_1

Fig. 8 shows the 144 differences (4 sample volumes, 3 flow rates, 2 needle seat capillaries I.D., 3 connecting tubes I.D., and presence or absence of heat exchanger) between the elution volumes recorded with a 2.4 and a 0.8 μL detection cell. The differences are all positive except one. It is noteworthy that this difference is larger than the average difference (1.18 μL, RSD = 47%) observed at a flow rate of 4.0 mL/min. The average difference measured by omitting those recorded at a flow rate of 4 mL/min is equal to 0.95 μL (RSD = 23%).

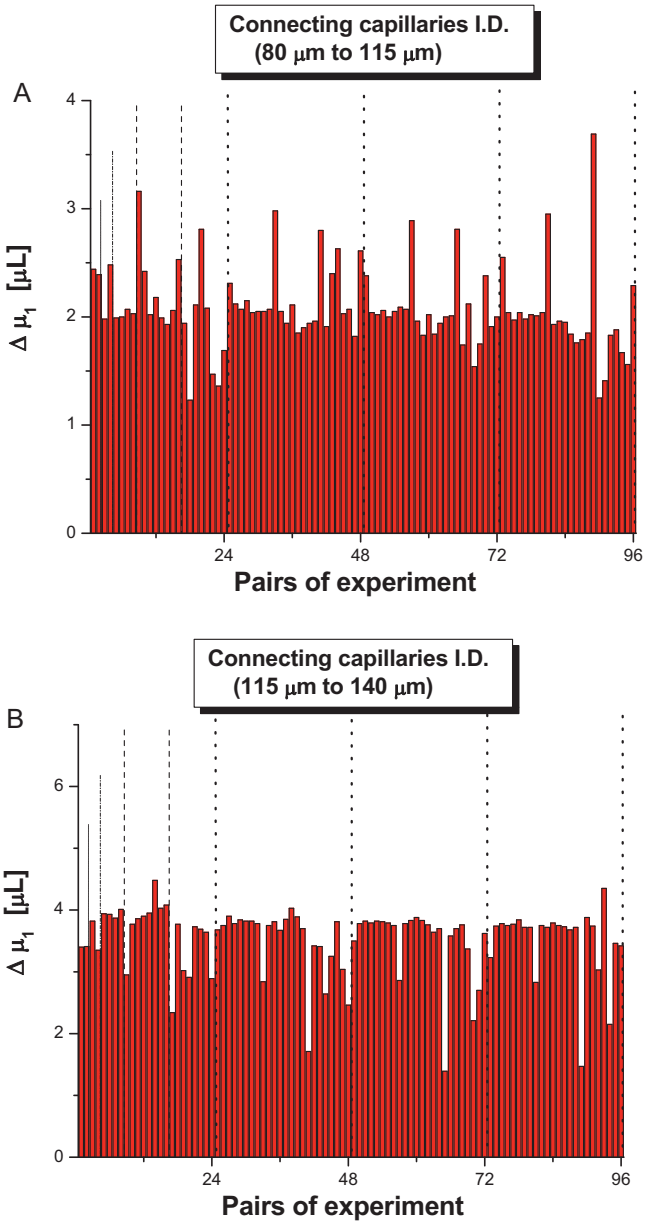

Fig. 7. (A) Impact of increasing the I.D. of the inlet and outlet connecting capillary tubes from 80 to 115 μm for 96 system configurations (4 injection volumes, 3 flow rates, 2 needle seat capillary I.D., 2 detection cell volumes, and the presence/absence of the heat exchanger) on the first moment observed. The average increase in the first moment is 2.08 μL. The *x*-axis is successively divided into 4 injection volumes, 3 flow rates, 2 needle seat capillary I.D., 2 detection cell volumes, and the presence/absence of the heat exchanger. (B) Same as in A, except increasing the I.D. of the connecting tubes from 115 μm to 140 μm The corresponding average increase in the first moment is 3.52 μL.

In theory, an increase of $(2.4-0.8)/2=0.8$ μL was expected. The measurements made at low flow rates (0.04 and 0.4 mL/min) are consistent with the volumes of the two detection cells provided by the manufacturer. The larger average values measured at 4 mL/min suggest that the large detection cell volume induces a severe peak tailing at high flow rates.

4.2.4. Presence/absence of the heat exchanger and μ_1

Fig. 9 shows the 144 differences (4 sample volumes, 3 flow rates, 2 needle seat capillaries I.D., 3 connecting tubes I.D., and 2 detection volumes) between the elution volumes recorded in the presence and in the absence of the heat exchanger. Similarly to what was

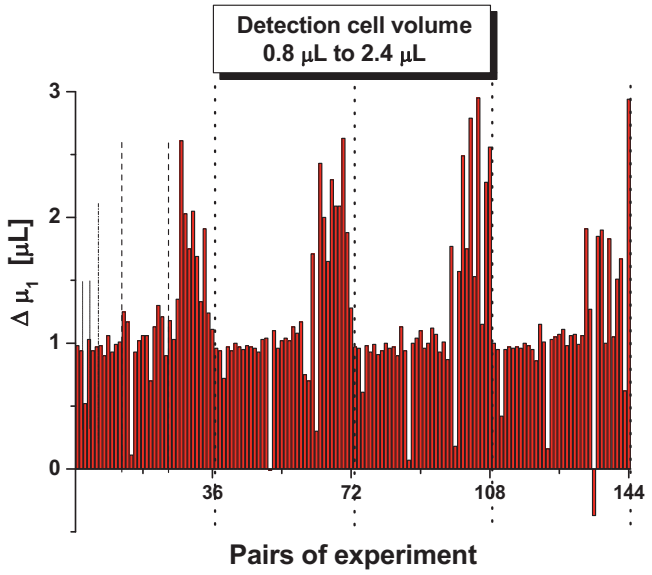

Fig. 8. Impact of increasing the I.D. of the detection cell volume from 0.8 to 2.4 µL for 144 system configurations on the first moment observed. The *x*-axis is successively divided into 4 injection volumes, 3 flow rates, 2 needle seat capillary I.D., 3 connecting tube I.D., and the presence/absence of the heat exchanger. The average increase in the first moment measured for the two lowest flow rates, only, is equal to 0.95 µL. Note the large excess in the first moment measured at the highest flow rate.

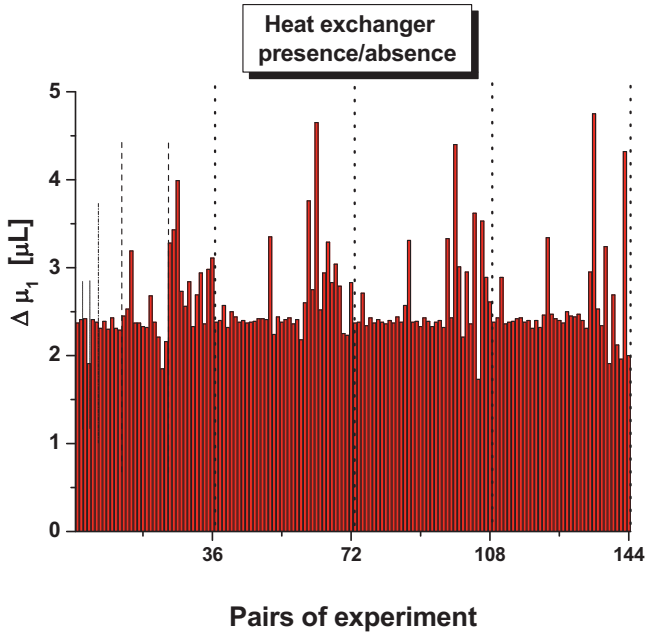

Fig. 9. Impact of the presence of the heat exchanger for 144 system configurations on the first moment observed. The *x*-axis is successively divided into 4 injection volumes, 3 flow rates, 2 needle seat capillary I.D., 3 connecting tube I.D., 2 detection cell volumes. The average increase in the first moment measured for the two lowest flow rates, only, is equal to 2.43 µL. Note the large excess in the first moment measured at the highest flow rate.

observed in the previous section, the differences observed between the values measured at the highest flow rate of 4 mL/min are larger than the average difference (2.59 µL, RSD = 19%). After omitting the data measured at 4 mL/min, the average difference is equal to 2.43 µL and the RSD is strongly decreased, to 9%. Surprisingly, the volume of the heat exchanger is only equal to 1.6 µL, according to the manufacturer. This could suggest either that the volume of the heat exchanger provided by the manufacturer is underestimated or that this exchanger contributes to a significant enhancement of peak tailing, which will be checked later, when analyzing the impact of the heat exchanger on the second central moments.

4.2.5. Sample volume and μ_1

The impact of the sample volume injected on the elution volume measured is illustrated in Fig. 10A through Fig. 10C, which show plots of the differences (72 pairs of experiments, e.g. 3 flow rates, 2 needle seat capillaries, 3 connecting tube capillaries, 2 detection cells, presence or absence of the heat exchanger, see the different styles of the solid lines in these figures) for different pairs of sample volumes, 0.16 and 0.80 µL, 0.80 and 4.0 µL, and 4.0 and 20.0 µL.

- Fig. 10A (0.16–0.80 µL). We observe that at high flow rates (0.4 and 4.0 mL/min), there are about as many positive as negative differences. The excessive peak tailing and the decrease in the precision of the measurements at these high flow rates do not allow the observation of the effect of a small increase of the injected volume on the first moment of the band profile. In contrast, at the lowest applied flow rate, 0.04 mL/min, where extra-column peak tailing is less pronounced, a positive difference is systematically observed for the 24 configurations of the instrument. The average difference is measured at 0.36 µL, for which the RSD is 32%. From the geometrical data, the shift in elution volume should be (0.80 − 0.16)/2 = 0.32 µL, which is consistent with the value measured.
- Fig. 10B (0.8–4.0 µL). In contrast to Fig. 10A, all the differences are positive because increasing the injected volume from 0.8 to 4.0 µL causes a significant and measurable increase in the first moment, even at the highest flow rate. Yet, we notice that the dispersion around the mean is larger at 4.0 mL/min than at 0.4 mL/min. The average difference at a flow rate of 0.04 mL/min is 1.70 µL with a RSD of only 2.4%. In theory, the shift in the elution volume should be (4.0 − 0.8)/2 = 1.6 µL, again consistent with the measured data.
- Fig. 10C (4.0–20.0 µL). For such a large increase of the injected volume, the differences are obviously positive at all flow rates and the values are more dispersed at 4.0 (RSD = 6.4%) than at either 0.04 (RSD = 0.9%) or 0.4 mL/min (RSD = 0.7%). The average difference in elution volume is 7.99 µL while the difference calculated from the geometrical volumes should be (20 − 4)/2 = 8.0 µL, practically equal.

In all three cases, the agreement between the expected and the measured shifts in the elution volumes is excellent, which demonstrates how accurate and reproducible the drawing and the delivery of the sample volume are with the sampling system of the 1290 Infinity system.

4.2.6. Flow rate and μ_1

We finally investigate the possible influence of the flow rate on the first moment, which, in principle should be negligible unless the tailing of the peak profiles is highly sensitive to the flow velocity. We assess here the differences between the first moments recorded at 0.4 and at 0.04 mL/min (Fig. 11A) and between those measured at 4.0 and at 0.4 mL/min (Fig. 11B). A total of 96 pairs of measurements are available for these comparisons (4 injection volumes, 2 needle seat capillaries, 3 connecting tube capillaries, 2 detection cell volumes, and the presence or absence of heat exchanger, see the different styles of the solid lines in these 2 figures).

- Fig. 11A (0.04–0.40 mL/min). The differences measured are all positive. Therefore, increasing the flow rate obviously impacts on the degree of peak asymmetry and leads to a measurable shift of the elution volume. Interestingly, A reveals that this

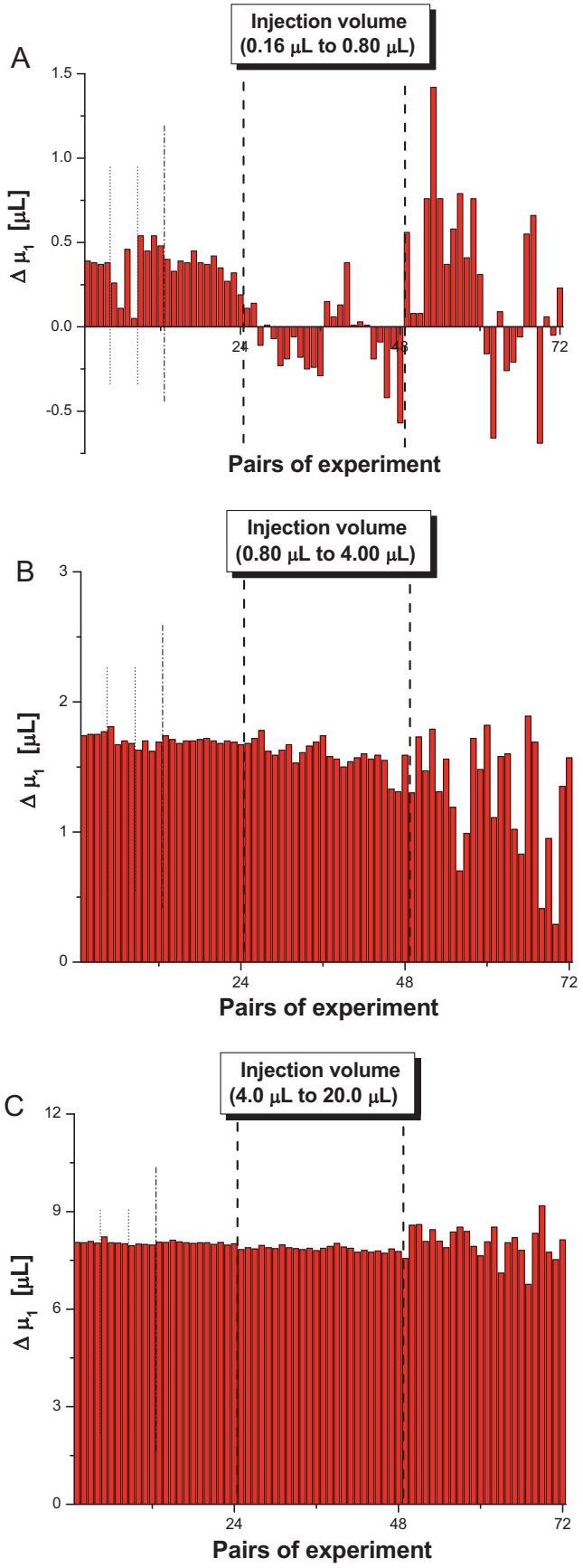

Fig. 10. (A) Impact of increasing the injected sample volume from 0.16 to 0.8 μL for 72 system configurations on the first moment observed. The *x*-axis is successively divided into 3 flow rates, 2 needle seat capillary I.D., 3 connecting tube I.D., 2 detection cell volumes, and the presence/absence of the heat exchanger. (B) Same as in A, except increasing the injected sample volume from 0.8 to 4.0 μL. (C) Same as in C, except increasing the injected sample volume from 4.0 to 20.0 μL. The average increases in the first moments recorded for the lowest flow rate, which minimizes peak tailing, are 0.36, 1.70, and 7.99 μL in A, B, and C, respectively.

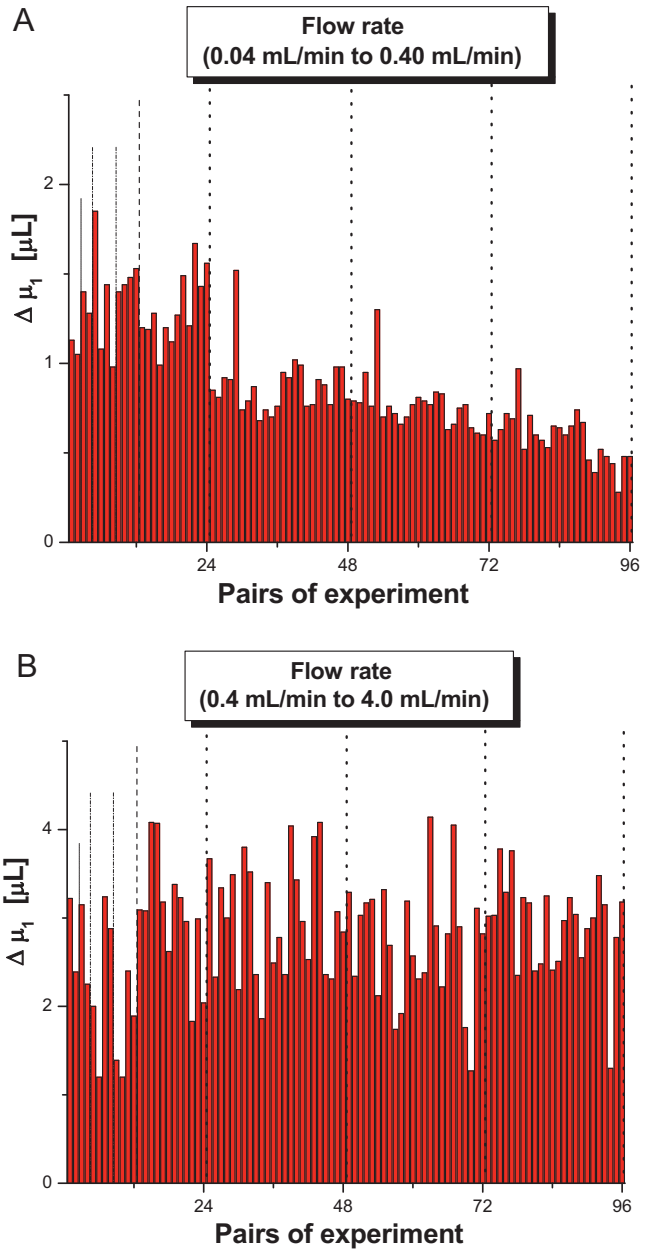

Fig. 11. Impact of increasing the flow rate from 0.04 to 0.40 mL/min for 96 system configurations on the first moment observed. The *x*-axis is successively divided into 4 injection volumes, 2 needle seat capillary I.D., 3 connecting tube I.D., 2 detection cell volumes, and the presence/absence of the heat exchanger. (B) Same as in A, except increasing the flow rate from 0.4 to 4.0 mL/min. The average increases in the first moment are equal to 0.89 and 2.83 μL in A and B, respectively.

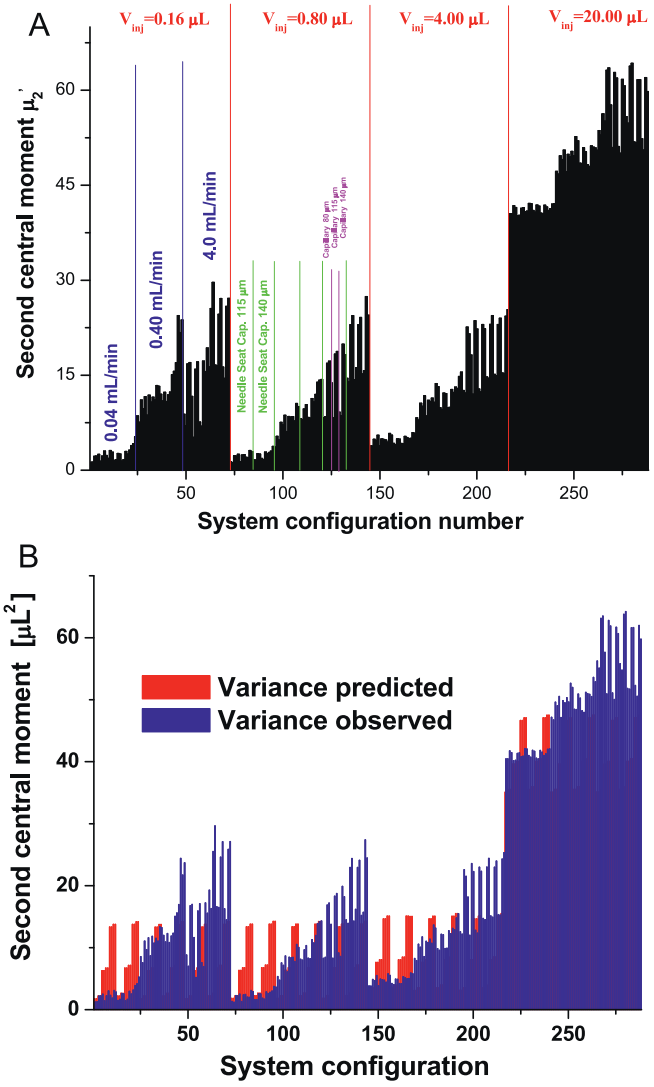

Fig. 12. (A) Plot of the experimental second central moments measured for the 288 system configurations. The *x*-axis is successively divided into 4 injection volumes, 3 flow rates, 2 needle seat capillary I.D., 3 connecting capillary tube I.D., 2 detection cell volumes, and the presence/absence of the heat exchanger. (B) Comparison between the observed and predicted variances of the extra-column band profiles of the 1290 Infinity system.

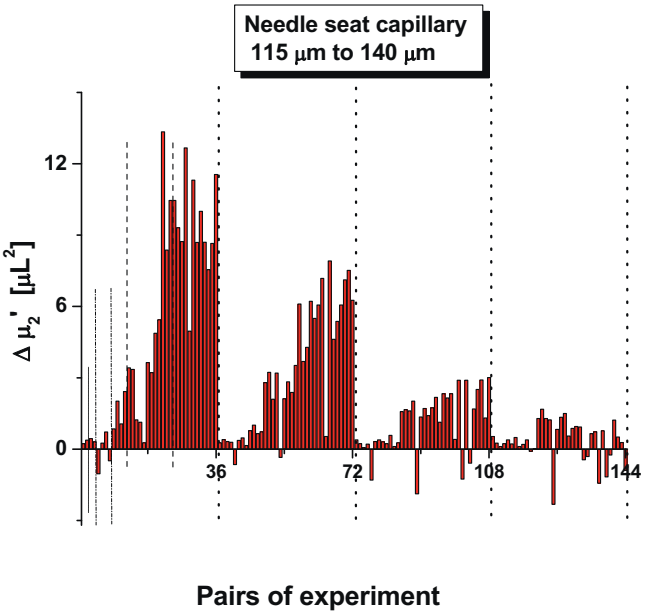

Fig. 13. Impact of increasing the I.D. of the needle seat capillary from 115 to 140 µm for 144 system configurations on the second central moment observed. The *x*-axis is successively divided into 4 injection volumes, 3 flow rates, 3 connecting tube I.D., 2 detection cell volumes, and the presence/absence of the heat exchanger. Note the significant impact at low injection volumes and high flow rates.

shift decreases from 1.32 (RSD = 26%) to 0.88 (RSD = 21%), 0.76 (RSD = 18%) and 0.58 µL (RSD = 30%) when the volume injected increases from 0.16 to 0.80, 4.0 and 20.0 µL.

- Fig. 11B (0.4–4.0 mL/min). Again, all the differences are positive. The tailing of the peak profiles increases further when the flow rate is increased from 0.4 to 4.0 mL/min. Yet, changing the sample volume does not affect much the results. The average difference is 2.83 µL with a RSD of 23%.

In conclusion, the flow rate affects the values of the first moments due to the enhanced tailing of the extra-column band profiles migrating along the tubings at high flow rates.

4.3. Analysis of the second central moment of the extra-column band profiles

Fig. 12A shows the averages (for 5 consecutive injections) of the second central moments expressed in volume squared unit, measured for the 288 system configurations described earlier. In the next sections, we assess the contributions to the overall second central moment due to changes of the characteristics of these configurations. The goal is to reveal from a statistical point of view, using a large number of system configurations, which are the critical parts of the 1290 Infinity instruments which provide large contributions to the extra-column band spreading.

The lowest value found for the second central moment was 1.22 µL^2, when using the parts having the smallest volumes, at the lowest flow rate (0.04 mL/min), and an injected volume of 0.8 µL. For the same injected volume, the largest peak variance was 27.43 µL^2 when using the parts with the largest volumes, at the highest flow rate (4.0 mL/min). According to Table 2, which provides the individual contributions to the band variance of the different parts of the instrument, it is possible to compare the values observed to those calculated, as shown in Fig. 12B. The smallest and largest predicted values are 1.84 and 14.28 µL^2, respectively. The first one is ca. 50% larger than the experimental value at low flow rate, suggesting that the variance calculation for connecting tubes gives overestimated values. In contrast, the second value is ca. half the observed one, suggesting that the calculations of some values in Table 2 do not properly account for the role of the flow rate on the variance and/or that some additional contributions were neglected (e.g., those of drawing/ejecting the sample, of the injection valve, the heat exchanger, and the anfractuosities). Strikingly, Fig. 12B shows that the influence of the inner diameter of the connecting tubes is weaker than expected for all injected volumes and all flow rates while the influence of the detector cell volume was clearly underestimated in the prediction provided by Eq. (7) for $K = 12$.

In the next sections, we analyze the impacts of each experimental parameter on the overall band variance contribution measured for the 1290 Infinity instrument.

4.3.1. Needle seat capillary I.D. and μ_2'

Fig. 13 shows the differences between the second central moments calculated for the 144 pairs of bands of naphthalene eluted through the instrument fitted with the 140 or the 115 µm

I.D. needle seat capillary tubes and having the same configuration, much like what was done for the first moment in Fig. 6.

Strikingly, these differences are very sensitive to the volume injected and to the flow rate applied. The largest differences are observed for the smallest volume injected and the largest flow rates, which corresponds to most conventional experimental conditions under ultra fast HPLC conditions. For instance, the average difference in the extra-column peak variance decreases from 9.4, 5.9, 1.7, to 0.0 μL^2 at 4 mL/min when the sample size varies from 0.16, 0.80, 4.0, to 20.0 μL. It decreases from 4.9, 3.0, 1.4, to 0.8 μL^2 and from 0.6, 0.4, 0.2, to 0.2 μL^2 at flow rates of 0.4 and 0.04 mL/min, respectively. In other words, the larger the sample size, the more reproducible the second moment of the peak, at all flow rates. This is not surprising because the larger sample size gives the larger signal to noise ratio in the regions remote from the band center, which contribute significantly to the second moment.

In conclusion, the influence of the needle seat capillary tube diameter on the extra-column peak variance is important when small sample volumes are injected at very high flow rates. Despite its short length (100 mm) relatively to that of the connecting tubes (560 mm), the needle seat capillary significantly affects the extra-column contribution to band broadening. Solutions aiming at eliminating the presence of this part from the system could help to reduce by ca. 4 to 6 μL^2 the extra-column band broadening contributions of sub-1 μL injections at high flow rates. This gain is of the order of magnitude of the variance expected for narrow-bore columns packed with sub-2 μm fully porous particles and/or sub-3 μm shell particles at a retention factor of 2. Alternately, by simple extrapolation, the use of a 80 μm needle seat capillary could be helpful in the future.

4.3.2. The inner diameter of the connecting tubes and μ_2'

Fig. 14A and B shows the impacts of increasing the inner diameter of the connecting tubes from 80 to 115 and from 115 to 140 μm to the extra-column peak variance contribution. In contrast to the influence of the diameter of these tubes on the first moment, there is no obvious systematic influence of this diameter on the second central moments, although there are significant effects under certain conditions. This impact depends strongly on the experimental conditions, making it difficult to propose a general rule. Yet, both figures reveal that the largest increases are observed when (1) the flow rate is intermediate (0.4 mL/min) and (2) the needle seat capillary diameter is 140 μm and (3) the sample volume is the smallest (0.16 μL). Clearly, increasing the I.D. of the connecting tubes does not have much impact on the peak variance observed at the highest flow rate (4 mL/min). In contrast and unexpectedly, we observe in Fig. 14B that, for all sample volumes, there is a strong, systematic decrease of the band variance for one particular system configuration, the one with a flow rate set at 4.0 mL/min, the I.D. of the needle seat capillary equal to 115 μm, with a 0.8 μL detection cell, and in presence of the heat exchanger.

In conclusion, in contrast to what was observed for the first moments (see Fig. 7A and B), the influence of the diameters of the connecting tubes on the overall peak variance is not straightforward. On the average, over 96 different system configurations, the second moment increases by only 0.4 and 1.1 μL^2 when the connecting tube diameter is increased from 80 to 115 and from 115 to 140 μm, respectively. In practice, connecting tubes with diameters smaller than 100 μm will not significantly decrease the variance contribution of the instrument. Worse, decreasing the diameters of these tubes at high flow rates can increase the peak variance. The diameter of the tubes currently used, 115 μm, seems to be the most reasonable compromise.

Alternative solutions that should be considered are (1) changing the architecture of the instrument, making it compact, and reducing the length of the connecting tubes needed between the injection device and the column and between the column and the detector cell; (2) replacing straight connecting tubes with twisted ones to enhance secondary circulation and radial dispersion, and to relax effectively the radial concentration gradients due to the Hagen–Poiseuille flow; (3) replacing the narrow open tubes currently used with wider tubes packed with fine, solid particles because such tubes would have much smaller variance contributions than open ones.

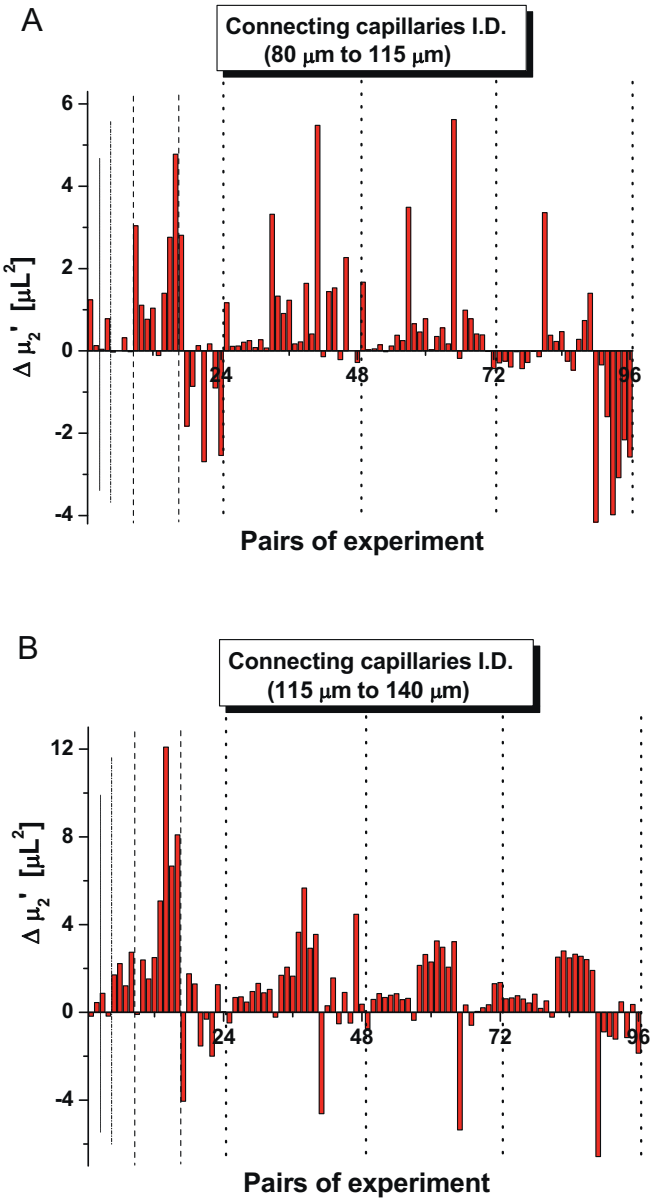

Fig. 14. (A) Impact of increasing the I.D. of the inlet and outlet connecting tube capillaries from 80 to 115 μm for 96 system configurations on the second central moment observed. The *x*-axis is successively divided into 4 injection volumes, 3 flow rates, 2 needle seat capillary I.D., 2 detection cell volumes, and the presence/absence of the heat exchanger. (B) Same as in A, except increasing the I.D. of the connecting tubes from 115 to 140 μm. Note the limited impact in most of the configurations.

4.3.3. Detection cell volume and μ_2'

Fig. 15 shows the effects of increasing the detection cell volume from 0.8 to 2.4 μL for the 144 system configurations studied. In contrast to what was observed in the previous section, the differences between the peak variances observed with pairs of data obtained with instrument configurations differing only by the detector cell

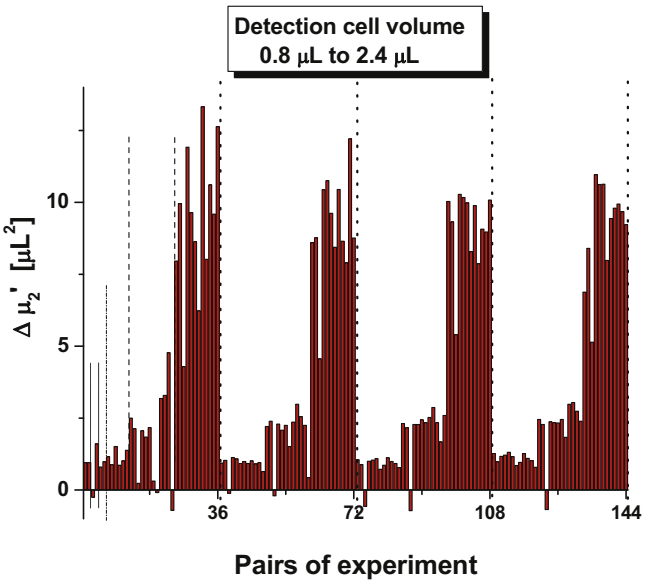

Fig. 15. Impact of increasing the I.D. of the detection cell volume from 0.8 to 2.4 µL for 144 system configurations on the second central moment observed. The *x*-axis is successively divided into 4 injection volumes, 3 flow rates, 2 needle seat capillary I.D., 3 connecting tube I.D., and the presence/absence of the heat exchanger. Note the increasing impact as the flow rate increases.

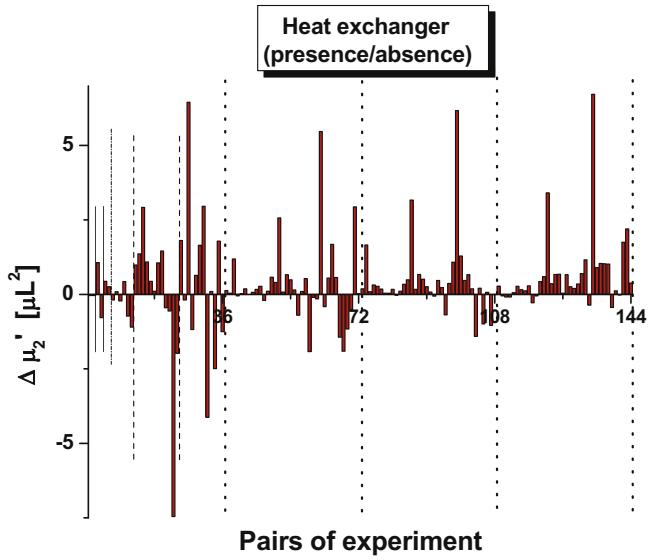

Fig. 16. Impact of increasing the presence of the heat exchanger for 144 system configurations on the second central moment observed. The *x*-axis is successively divided into 4 injection volumes, 3 flow rates, 2 needle seat capillary I.D., 3 connecting tube I.D., 2 detection cell volumes. Note the very limited impact for most configurations.

are nearly all positive. This contrast is worth noting because the difference between the volumes of the sets of connecting tubes was as large as 3.0 and 2.8 µL while the difference between the cell volumes is only 1.6 µL. Yet, the impact of changing the cell volume of the detector on the band variance is much larger than that of changing the volume of the connecting tubes.

The variance contribution of the instrument due to the detector cell volume depends considerably on the mobile phase flow rate, far more than that of the connecting tube volume. A simple model of the variance contribution due the sole increase of the volume of this cell is given by

$$\Delta\sigma^2_{v,cell} = \frac{2.4^2 - 0.8^2}{12} = 0.43\mu L^2 \quad (16)$$

On the average, the measured values for $\Delta\sigma^2_{v,cell}$ are 0.94, 2.01, and 9.17 µL^2 at flow rates of 0.04, 0.4, and 4.0 mL/min, respectively. These variances are larger than those calculated from Eq. (16), which shows that the factor $K = 12$ should be replaced with a value between 5 and 6 for the lowest flow rates and that some extra band broadening effects take place at high flow rates in the detector cell. The lower volume of the detection cell is achieved by reducing the cell diameter and keeping constant its path length. Eq. (5) accounts for the variance expected for a short capillary tube of length L, inner radius r_c, and flow rate F_v. The path length is equal to $L = 10$ mm, the inner radii are equal to $r_c = 276$ µm (2.4 µL cell) and 160 µm (0.8 µL cell). The variance increments predicted by Eq. (5) are 1.15, 1.62, and 1.69 µL^2. Whereas these predictions are consistent with the observations made at low flow rates, they underestimate the experimental values at high flow rates.

Note also that the dependence of the second moments on the flow rate observed is not affected by the sampling rate of the detector signal. Table 2 lists the contributions of this sampling rate at flow rates of 0.04, 0.40, and 4.0 mL/min. They are all smaller than 0.01 µL^2. Thus, it is of major importance to keep the cell volume as small as possible when fast analyses are performed and high flow rates used.

4.3.4. Presence/absence of the Heat exchanger and μ_2'

Fig. 16 shows the 144 differences between the variance contributions recorded in the presence and in the absence of the heat exchanger. In contrast to Fig. 15, there is no obvious increase in the peak variance when the heat exchanger is inserted between the inlet and the outlet capillary. This might seem surprising because its volume (1.6 µL) is the same as the difference between the volumes of the two detector cells (2.4 − 0.8 = 1.6 µL). However, a significant increase of this variance (+6 µL^2) was observed for all injected volumes at 4 mL/min and with the 115 µm needle seat capillary. This isolated case could well be the result of a measurement failure. On the average, the peak variance increases only by 0.12, 0.35, and 0.68 µL^2 at flow rates of 0.04, 0.4, and 4.0 mL/min, respectively, showing an impact nearly one order of magnitude less than that observed with the change in the UV cell volume.

4.3.5. Sample volume and μ_2'

The influence of an increase in the sample volume injected on the observed peak variance is illustrated in Fig. 17A to C, which show the differences in the second central moments for 72 pairs of experiments (3 flow rates, 2 needle seat capillaries, 3 connecting tube capillaries, 2 detection cells, presence or absence of the heat exchanger, see the different styles of the solid lines in these figures) when the sample volumes is increased from 0.16 to 0.80, 0.80 to 4.0, and 4.0 to 20.0 µL.

- In Fig. 17A (0.16–0.80 µL), we observe that increasing the sample volume from 0.16 to 0.80 µL at the low flow rate (0.04 mL/min) has no measurable effect, given the accuracy and the precision of the measurements of the second moments. In contrast, at a flow rate of 0.4 mL/min, increasing this volume considerably decreases the extra-column variance contribution. This effect is particularly important with the 140 µm needle seat capillary, which is apparently inconsistent with the increase of the injected plug variance, which can be calculated to be $(0.8^2 - 0.16^2)/12 = +0.05\mu L^2$. In contrast, the average decrease observed is −3.93 µL^2. This observation is probably explained by the higher concentration gradients associated with larger injection volumes, which allow faster radial mass transfers and a

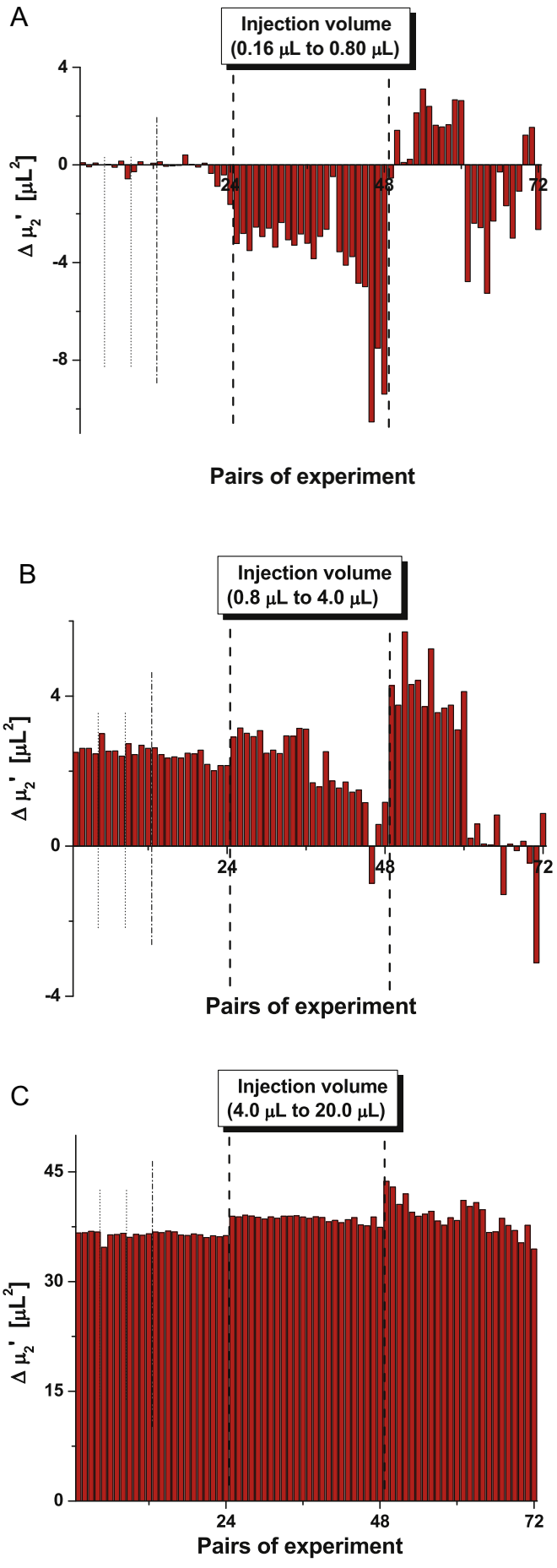

significant diminution in the extra-column variance contribution. Finally, at the large flow rate of 4 mL/min, the results are different again. The variances increase and decrease when the 115 and 140 μm needle seat capillary tubes are used in the system. This suggests that concentration gradients control band broadening to a lesser degree than velocity gradients.

- Fig. 17B illustrates the effect of increasing the sample volume from 0.80 to 4.00 μL. The increase in the extra-column variance is now measurable at the smallest flow rate of 0.04 mL/min. On the average, this increase is +2.47 μL^2 while calculation would predict $(4.0^2 - 0.8^2)/12 = +1.28\ \mu L^2$. The average increase is +4.14 μL^2 at a flow rate of 4 mL/min, with the 115 μm I.D. needle seat capillary. Thus, the value measured is twice larger the one expected, suggesting that the profile of the sample volume injected is far from the ideal rectangular plug. Interestingly, in agreement with the observation made for Fig. 17A, the increase in the peak variance is less when the 140 μm I.D. needle seat capillary is used. The average increases of the peak variance drop to +1.30 μL^2 (+2.47 μL^2 with the 115 μm needle seat capillary) to −0.18 μL^2 (+4.14 μL^2 with the 140 μm I.D. needle seat tube). This correlation between the volume injected and the diameter of the needle seat capillary was not expected.
- Fig. 17C shows the effect of an increase from 4.0 to 20.0 μL of the injected volume. For such a large increase, the differences are nearly independent of the flow rate and the diameter of the needle seat capillary. Still, one can detect a slight influence of the needle seat capillary diameter at the highest flow rates of 0.4 and 4.0 mL/min. The average increase in peak variance observed at a flow rate of 0.04 mL/min is 36.4 μL^2. Based on geometry, we would have expected a value of $(20^2 - 4^2)/12 = 32\ \mu L^2$. The excess of 4 μL^2 is a measure of the distance that separates the actual injection system of the 1290 instrument from an ideal injector that would provide rectangular injection profiles.

This section demonstrates that it should be possible to improve the performance of the injection systems of chromatographic instruments by modifying them, if possible, so that they would provide injection profiles closer to a rectangular plug.

4.3.6. Flow rate and μ_2'

The influence of the flow rate on the values of the second central moment of the extra-column contribution to band broadening is due to the influence that the flow rate has on the shapes of the peak profiles, due to the increase of the radial flow gradient with increasing flow rate. This increase results in an enhanced peak tailing, which is expected to provide larger peak variances. For each increment in flow rate, a total of 96 pairs of experiments are available (4 injection volumes, 2 needle seat capillaries, 3 connecting tube capillaries, 2 detection cell volumes, and the presence or absence of heat exchanger, see the different styles of the solid lines in these 2 figures).

- We observe in Fig. 18A (0.04–0.40 mL/min) that the differences between the variances are positive and are essentially controlled by the extra-column volume of the system. The larger the diameter of the needle seat capillary, the larger the connecting tube diameter, and the larger the detector cell volume, the larger the rate of increase of the peak variance with increasing flow rate.

Fig. 17. (A) Impact of increasing the injected sample volume from 0.16 to 0.8 μL for 72 system configurations on the second central moment observed. The *x*-axis is successively divided into 3 flow rates, 2 needle seat capillary I.D., 3 connecting tube I.D., 2 detection cell volumes, and the presence/absence of the heat exchanger. (B) Same as in A, except increasing the injected sample volume from 0.8 to 4.0 μL. (C) Same as in A, except increasing the injected sample volume from 4.0 to 20.0 μL.

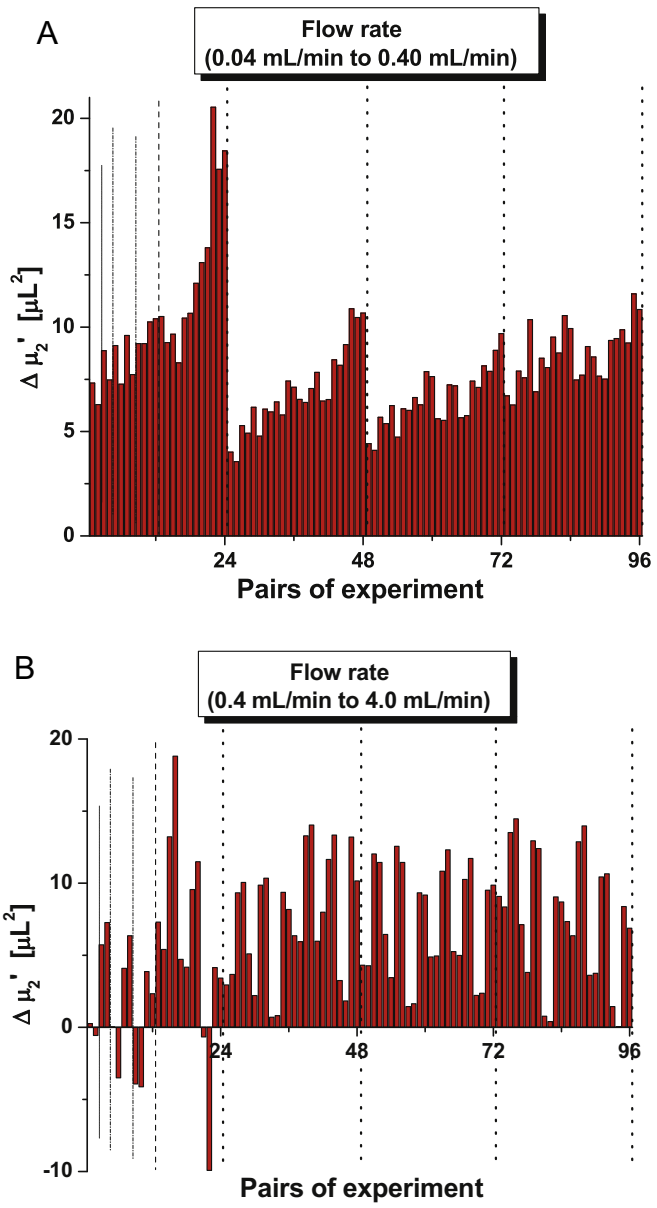

Fig. 18. (A) Impact of increasing the flow rate from 0.04 to 0.40 mL/min for 96 system configurations on the second central moment observed. The *x*-axis is successively divided into 4 injection volumes, 2 needle seat capillary I.D., 3 connecting tube I.D., 2 detection cell volumes, and the presence/absence of the heat exchanger. (B) Same as in A, except increasing the flow rate from 0.4 to 4.0 mL/min. The average increases in the first moment are equal to 0.89 and 2.83 μL in Fig. 11A and B, respectively.

The same observation is made in the presence or absence of the heat exchanger. This increase is particularly large with the smallest injected volume (0.16 μL), meaning when the concentration gradients are the lowest. The average increases are 10.7, 6.9, 6.5, and 8.7 μL^2 for injected sample volumes of 0.16, 0.80, 4.0, and 20 μL, respectively.

- Fig. 18B (0.4–4.0 mL/min). When increasing 10-fold further the flow rate, from 0.4 to 4.0 mL/min, we observe a systematic, significant increase of the band variance when the 2.4 μL detection cell is used. This result might be explained by turbulence and eddies taking place at the inlet of the cell, due to the abrupt change in the channel cross-section area. It shows the importance of choosing a low detection cell volume when operating at very high flow rates. The average increase of the band variances are +3.0 and +10.2 μL^2 for detection cell volumes of 0.8 and 2.4 μL, respectively.

In conclusion, the flow rate essentially affects the values of the second central moments when the detector cell used has a large volume, the flow rate is high, and, more generally, when the first moment of the extra-column volume is large.

5. Conclusion

In summary, we showed that the extra-column volume of an HPLC instrument induces a significant band broadening contribution for the elution peaks of samples of a dilute solution of naphthalene (<0.1 g/L). We measured this contribution for 288 different system configurations of an Agilent 1290 Infinity HPLC system, including 4 sample volumes (0.16, 0.80, 4.0, and 20.0 μL), 3 flow rates (0.04, 0.40, and 4.0 mL/min), 2 needle seat capillary I.D., 3 connecting tube capillaries I.D., 2 detector cell volumes, and in the presence/absence of the heat exchanger. A detailed analysis of these contributions leads to the following conclusions.

- The first moments are systematically 30% larger than the sum of the volume contributions calculated for all the parts of the instrument, based on their geometrical dimensions. This delay is most likely caused by imperfections in the delivery of the rear part of the sample volume and/or by the presence of anfractuosities in the channel walls, both contributing also to increase the peak tailing.
- The diameter of the needle seat capillary tubes should be kept small when small sample volumes are injected (<1 μL) and when the flow rate is large (>1 mL/min). Because the length of the needle seat tube is short (100 mm), 80 μm needle seat capillary tubes with the proper injection needle give a small band broadening contribution, particularly at low flow rates.
- Minimizing the diameter of the connecting tubes is advantageous only at low flow rates (<0.1 mL/min) and when the diameter of the needle seat capillary is large (140 μm). More generally, minimizing the diameters of these tubings while keeping small the diameter of the needle seat capillary does not necessarily provide significantly smaller variances contributions. Therefore, sub-100 μm I.D. connecting tubes are not more advantageous than 100–140 μm I.D. tubes. It could be possible to reduce the band broadening contributions of these tubes by filling them with a highly permeable silica monolith with no secondary porosity (i.e., nonporous "porons") in order to eliminate the radial Hagen–Poiseuille flow profile.
- The detector cell volume seems to be the part of the instrument that affects the instrument variance contribution the most. It is strongly flow rate dependent. Minimizing this volume (e.g., from 2.4 → 0.8 μL) is critical at high flow rates ($-7\mu L^2$ at 4 mL/min, $-2\mu L^2$ at 0.4 mL/min, and $-1\mu L^2$ at 0.04 mL/min). Using a 500 nL detector cell could further improve the performance of instruments.
- The presence of the heat exchanger has nearly no impact on the variance measured for all flow rates. This suggests that this part was well designed to minimize its extra-column contribution once inserted in the flow path.
- On the one hand, the sample volume should be kept small to avoid volume overload of the column. On the other hand, it should be large enough to maximize the concentration gradients across the extra-column tubes, hence their rate of radial equilibration. It was observed that the injection system is far from ideal. The excess variance contribution is at least 4 μL^2. It could be reduced by using a better injection system which would shorten the rear part of the delivered sample band.
- Finally, the flow rate should be kept as small as possible to maintain the radial velocity gradients across the capillaries' diameter

as small as possible. Admittedly, this is not consistent with the desire of most analysts to achieve high throughputs.

We are planning to test shortly the performance of our instrument modified by replacement of some of the most critical parts discussed above with others of an improved design and to assess the validity of our conclusions based on the measurements reported here.

Acknowledgements

This work was supported in part by the cooperative agreement between the University of Tennessee and the Oak Ridge National Laboratory. We thank Gerard Rozing, Monika Dittman, and Bill Arnold (Agilent Technologies) for the loan of the 1290 Infinity HPLC system instrument and for many fruitful discussions.

References

[1] U. Neue, N. Brady, S. Serpa, P. Iraneta, B. Alden, T. Walter, K. Wyndham, 32nd International Symposium on High Performance Liquid Phase Separations and Related Techniques, Baltimore, MD, May 10–16, 2008.
[2] F. Gritti, G. Guiochon, J. Chromatogr. A 1216 (2009) 1353.
[3] F. Gritti, G. Guiochon, J. Chromatogr. A 1217 (2010) 1485.
[4] J.J. Kirkland, Anal. Chem. 64 (1992) 1239.
[5] F. Gritti, G. Guiochon, J. Chromatogr. A 1157 (2007) 289.
[6] J.J. DeStefano, T.J. Langlois, J.J. Kirkland, J. Chromatogr. Sci. 46 (2008) 254.
[7] F. Gritti, I. Leonardis, D. Shock, P. Stevenson, A. Shalliker, G. Guiochon, J. Chromatogr. A 1217 (2010) 1589.
[8] F. Gritti, G. Guiochon, J. Chromatogr. A 1217 (2010) 1604.
[9] F. Gritti, I. Leonardis, J. Abia, G. Guiochon, J. Chromatogr. A 1217 (2010) 3219.
[10] S.A. Schuster, B.M. Wagner, B.E. Boyes, J.J. Kirkland, J. Chromatogr. Sci. 48 (2010) 566.
[11] E. Olah, S. Fekete, J. Fekete, K. Ganzler, J. Chromatogr. A 1217 (2010) 3642.
[12] Y. Zhang, X. Wang, P. Mukherjee, P. Petersson, J. Chromatogr. A 1216 (2010) 4597.
[13] F. Gritti, G. Guiochon, J. Chromatogr. A 1217 (2010) 7677.
[14] H. Lin, C. Horváth, Chem. Eng. Sci. 36 (1981) 47.
[15] H. Poppe, J. Kraak, J. Huber, H. van der Berg, Chromatographia 36 (1981) 515.
[16] U. Neue, M. Kele, J. Chromatogr. A 1149 (2007) 236.
[17] F. Gritti, G. Guiochon, J. Chromatogr. A 1187 (2008) 165.
[18] F. Gritti, G. Guiochon, Anal. Chem. 80 (2008) 5009.
[19] F. Gritti, G. Guiochon, Anal. Chem. 80 (2008) 6488.
[20] F. Gritti, G. Guiochon, J. Chromatogr. A 1138 (2007) 141.
[21] F. Gritti, G. Guiochon, J. Chromatogr. A 1166 (2007) 47.
[22] F. Gritti, M. Martin, G. Guiochon, Anal. Chem. 81 (2009) 3365.
[23] F. Gritti, G. Guiochon, J. Chromatogr. A 1217 (2010) 5069.
[24] F. Gritti, G. Guiochon, Chem. Eng. Sci. 65 (2010) 6310.
[25] C. Gritti, F. Sanchez, T. Farkas, G. Guiochon, J. Chromatogr. A 1217 (2010) 3000.
[26] J. Sternberg, Advances in Chromatography, Marcel Dekker, New York, NY, 1966.
[27] K.J. Fountain, U.D. Neue, E.S. Grumbach, D.M. Diehl, G. Guiochon, J. Chromatogr. A 1216 (2010) 5979.
[28] R. Aris, Proc. R. Soc. A 235 (1956) 67.
[29] M. Golay, J. Atwood, J. Chromatogr. 186 (1979) 353.
[30] C. Wilke, P. Chang, AIChE J. 1 (1955) 264.
[31] J. Giddings, Dynamics of Chromatography, Marcel Dekker, New York, NY, 1965.
[32] F. Gritti, G. Guiochon, J. Chromatogr. A, in press, doi:10.1016/j.chroma.2011.05.035.
[33] G. Guiochon, A. Felinger, A. Katti, D. Shirazi, Fundamentals of Preparative and Nonlinear Chromatography, 2nd ed., Academic Press, Boston, MA, 2006.
[34] H. Lauer, G. Rozing, Chromatographia 14 (1981) 641.